ACCEPTED MANUSCRIPT

AIP Advances

This is the author's peer reviewed, accepted manuscript. However, the online version of record will be different from this version once it has been copyedited and typeset.
PLEASE CITE THIS ARTICLE AS DOI:10.1063/5.0009554

Representation of anisotropic magnetic characteristic observed in a non-oriented silicon steel sheet

B. Upadhaya,[1, a)] L. Perkkiö,[2, b)] P. Rasilo,[3, c)] A. Belahcen,[1] P. Handgruber,[4] and A. Arkkio[1]

[1)]*Department of Electrical Engineering and Automation, Aalto University, FI-00076 Espoo, Finland*

[2)]*Department of Mathematics and Systems Analysis, Aalto University, FI-00076 Espoo, Finland*

[3)]*Unit of Electrical Engineering, Tampere University, FI-33014 Tampere, Finland*

[4)]*Institute of Fundamentals and Theory in Electrical Engineering, Graz University of Technology, Graz, A-8010, Austria*

(Dated: May 28, 2020)

This article presents a modified Jiles-Atherton hysteresis model for a weakly anisotropic non-oriented silicon steel sheet. In a toroidal inductor, the magnetic flux density can point towards any direction compared to the sheet orientation, and the hysteresis model should take this into account. We identify the model parameters independently for unidirectional alternating $B(H)$-characteristics in seven different directions. Then, we construct an anisotropic hysteresis model, where the model parameters can depend on the magnitude and direction of the applied magnetic flux density. We demonstrate that the parameters identified in the rolling and transverse directions of the silicon steel sheet (M400-50A) are sufficient to describe the hysteresis losses in other directions.

[a)]brijesh.upadhaya@aalto.fi

[b)]lauri.perkkio@aalto.fi

[c)]paavo.rasilo@tuni.fi

ACCEPTED MANUSCRIPT

AIP Advances

This is the author's peer reviewed, accepted manuscript. However, the online version of record will be different from this version once it has been copyedited and typeset.
PLEASE CITE THIS ARTICLE AS DOI:10.1063/5.0009554

AIP Publishing

I. INTRODUCTION

In this article, we aim to model the anisotropic magnetic behavior of non-oriented (NO) silicon steel sheet by a modified Jiles-Atherton (J-A) hysteresis model. NO silicon steel is widely used as a magnetic core material in toroidal inductors, rotating electrical machines, and several other electromagnetic devices, and several studies confirm that the material presents a significant level of magnetic anisotropy[1,2]. The anisotropy in the core affects the performance of an electromagnetic device[3,4], so it is essential to account for this effect in the magnetic hysteresis model[5,6].

The Jiles-Atherton (J-A) hysteresis model[7,8] is widely used to model polycrystalline electrical steels, such as NO and grain-oriented (GO) silicon steels[7,9,10]. Compared with the Preisach type hysteresis models[11], the J-A model has a simple mathematical formulation. In particular, the number of involved parameters is minimal compared to the Preisach model. The J-A model lack memory property (as opposed to the Preisach type and energy-based[12] models). Consequently, non-symmetric minor loops are not exactly closed[13]. Also, it is not well understood if the J-A model can represent both the alternating and rotational magnetic field variations simultaneously[14–16]. However, if non-closed minor loops and a rotational magnetic field are not a concern, then the $B(H)$-characteristics can be modeled efficiently with the J-A model[13,17]. Moreover, the model has been found to be suitable in studying the effect of external mechanical stress on the $B(H)$-characteristics of a soft-magnetic material[18].

The J-A model is usually presented with isotropic, fixed parameters. Several studies show that M (or H or B)-dependent model parameters produce a better fit with the measured symmetric minor and major hysteresis loops[19–24]. In an attempt to introduce anisotropy into the modified J-A model, the authors in Ref. 14 and Ref. 25 identify separate parameters for $B(H)$-loops measured in the rolling (RD) and transverse (TD) directions, and "interpolate" the models in the intermediate directions. Their extended J-A model, however, does not take into account the directional variation of the parameters. We claim that in devices like toroidal inductors, the anisotropic J-A model with parameters from RD and TD alone does not accurately describe the more complicated unidirectional alternating $B(H)$-characteristics. As we discuss in Section-II, the anhysteretic magnetization, as well as the hysteresis losses, vary according to the direction of applied magnetic flux density[10]. Thus, it is important to consider a more detailed directional variation of the J-A model parameters.

In this work, we first identify the J-A model parameters for unidirectional alternating $B(H)$-

ACCEPTED MANUSCRIPT
AIP Advances
This is the author's peer reviewed, accepted manuscript. However, the online version of record will be different from this version once it has been copyedited and typeset.
PLEASE CITE THIS ARTICLE AS DOI:10.1063/5.0009554
AIP Publishing

characteristics in seven different measurement directions. Secondly, we show that the identified parameters can be said to depend on both the magnitude and direction of the input excitation. Thirdly, we express the identified (magnitude- and direction-dependent) anisotropic parameters with analytical functions. Finally, we demonstrate that the augmented model gives a better fit with observed $B(H)$-characteristics of a weakly anisotropic NO silicon steel sheet (M400-50A).

II. METHODOLOGY

A. J-A hysteresis model

The J-A model gives the relation between B and H as a differential equation $\mathrm{d}B/\mathrm{d}H$, known as the differential permeability. The original derivation of the model is presented in Refs. 7 and 8. In this work, we consider the inverse J-A model, where B is the input variable[25,26]. The inverse J-A model is presented in the following.

The bulk magnetization is assumed to be of form

$$M = M_{\mathrm{rev}} + M_{\mathrm{irr}}, \tag{1}$$

$$M_{\mathrm{rev}} = c\left(M_{\mathrm{an}} - M_{\mathrm{irr}}\right), \tag{2}$$

$$M_{\mathrm{irr}} = \frac{M - cM_{\mathrm{an}}}{1-c}, \tag{3}$$

where M_{an}, M_{irr}, and M_{rev} represent the anhysteretic, irreversible, and reversible magnetizations, respectively. The dimensionless parameter c is the representative of domain wall bowing[7].

For an isotropic magnetic material, the anhysteretic magnetization is usually given as

$$M_{\mathrm{an}}(H_{\mathrm{eff}}) = M_{\mathrm{s}} L\left(\frac{H_{\mathrm{eff}}}{a}\right), \tag{4}$$

$$L(x) = \coth(x) - \frac{1}{x}, \tag{5}$$

$$H_{\mathrm{eff}} = H + \alpha M, \tag{6}$$

$$B = \mu_0\left(H + M\right), \tag{7}$$

where M_{s} represents the technical saturation magnetization, L is the so-called Langevin function[27], H_{eff} represents the effective field strength, which is composed of the applied field strength H and the interaction field strength αM, a modifies the shape of the anhysteretic curve, which is primarily a function of temperature, α represents the inter-domain coupling, and μ_0 is the permeability of free space.

ACCEPTED MANUSCRIPT
AIP Advances
This is the author's peer reviewed, accepted manuscript. However, the online version of record will be different from this version once it has been copyedited and typeset.
PLEASE CITE THIS ARTICLE AS DOI:10.1063/5.0009554
AIP Publishing

The inverse J-A model is written as a first-order differential equation[26],

$$\frac{\mathrm{d}M}{\mathrm{d}B} = \begin{cases} \dfrac{c\xi}{\mu_0\left[1+c\xi(1-\alpha)\right]}, & \text{if } (M_{\mathrm{an}} - M_{\mathrm{irr}})\mathrm{d}H_{\mathrm{eff}} \leq 0, \\ \dfrac{(1-c)\chi + c\xi}{\mu_0\left[1+(1-c)\chi(1-\alpha)+c\xi(1-\alpha)\right]} & \text{otherwise}, \end{cases} \tag{8}$$

where k is a pinning parameter corresponding to the average density of the pinning sites, and χ and ξ represent the differential irreversible and differential anhysteretic susceptibilities,

$$\chi = \frac{\mathrm{d}M_{\mathrm{irr}}}{\mathrm{d}H_{\mathrm{eff}}} = \frac{|M_{\mathrm{an}} - M_{\mathrm{irr}}|}{k}, \qquad \xi = \frac{\mathrm{d}M_{\mathrm{an}}}{\mathrm{d}H_{\mathrm{eff}}}.$$

Finally, the differential reluctivity is obtained using the constitutive relationship (7), and (8):

$$\frac{\mathrm{d}H}{\mathrm{d}B} = \frac{1}{\mu_0} - \frac{\mathrm{d}M}{\mathrm{d}B}. \tag{9}$$

Given the initial states H_{t} and B_{t}, and the excitation $B_{\mathrm{t}+\Delta\mathrm{t}}$, the field strength $H_{\mathrm{t}+\Delta\mathrm{t}}$ is solved from the differential equation (9) numerically by an explicit fourth-order Runge-Kutta (RK4) method[28].

B. Measurement of *B(H)* characteristic

The measured unidirectional alternating $B(H)$-characteristics used in this paper are obtained from a 0.5 mm thick NO silicon steel sheet of grade M400-50A. The quasi-static magnetic measurements are performed using a single sheet tester; for details, see Refs. 6 and 29. We utilize $B(H)$ measurements from seven directions (0°, 15°, 30°, 45°, 60°, 75°, 90°). For each measurement direction, the several $B(H)$ curves are measured with the peak amplitudes of B being 0.1 T, 0.2 T, 0.3 T, …, 1.5 T.

The measured $B(H)$-characteristics in seven different directions with respect to (w.r.t.) the RD are shown in Fig. 1. In Fig. 1a, the RD (0°) and TD (90°) alternating fields are shown; Fig. 1b depicts alternating fields in 15° and 75° directions; Fig. 1c depicts alternating fields in 30° and 60° directions; Fig. 1d depicts alternating fields in 45° direction, and average $B(H)$-characteristics of all seven directions. The result shows that the NO silicon steel requires different values of field strength H to reach the same value of flux density B in seven different directions. Hence, the measurement result verify that the NO silicon steel of grade M400-50A is magnetically anisotropic.

ACCEPTED MANUSCRIPT
AIP Advances
This is the author's peer reviewed, accepted manuscript. However, the online version of record will be different from this version once it has been copyedited and typeset.
PLEASE CITE THIS ARTICLE AS DOI:10.1063/5.0009554
AIP Publishing

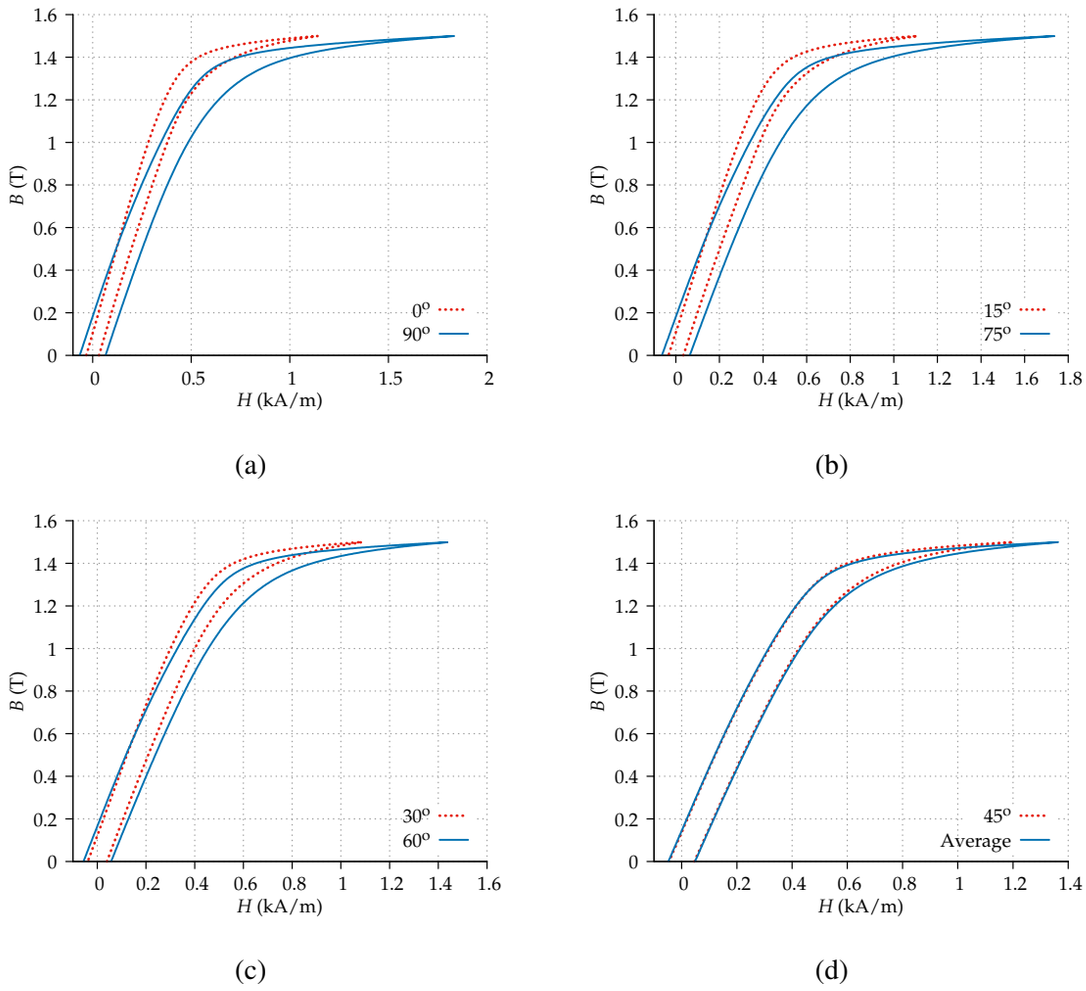

Figure 1: Measured $B(H)$-loops of M400-50A. (a) 0° (RD) and 90° (TD). (b) 15° and 75°. (c) 30° and 60°. (d) 45°, and the average of all seven directions.

C. Anhysteretic magnetization

The anisotropy in the J-A model is normally introduced in the anhysteretic magnetization curve[9,10,16,30,31]. When modeling NO silicon steel, the modified Langevin function (5) is commonly used to represent the anhysteretic magnetization[7,32]. Depending on the magnetic material type, several other functions have been proposed and utilized[7,31,33–35].

In this work, we do not utilize a closed-form function to model the anhysteretic magnetization. Instead, we assume that averaging the field strength of the ascending and descending branches of the major hysteresis loop gives a reasonable estimate of the anhysteretic magnetization[36]. The uncritical use of phenomenological dependence, i.e., modified Langevin function, might lead to

ACCEPTED MANUSCRIPT
AIP Advances
This is the author's peer reviewed, accepted manuscript. However, the online version of record will be different from this version once it has been copyedited and typeset.
PLEASE CITE THIS ARTICLE AS DOI:10.1063/5.0009554
AIP Publishing

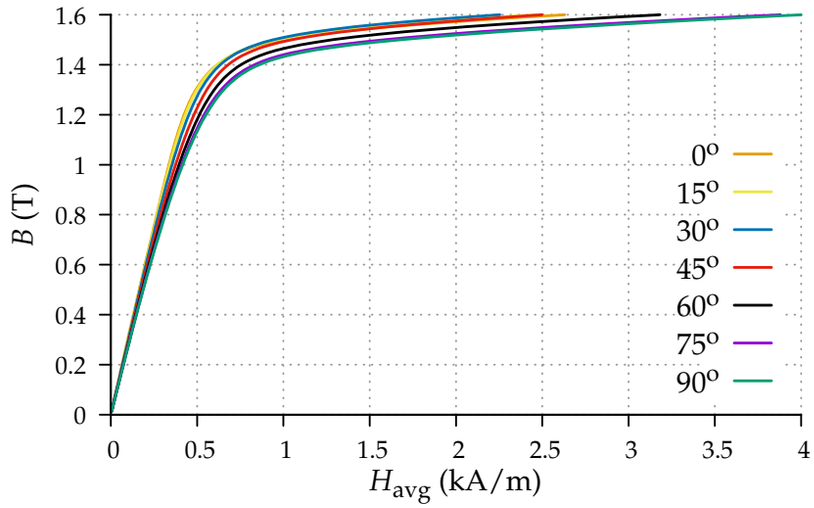

Figure 2: Anhysteretic magnetization curves of M400-50A, obtained for seven different measurement directions w.r.t the RD.

serious problems for certain sets of model parameters[37]. The $M(H_{\text{avg}})$ curve obtained by averaging the major hysteresis loop is expressed as a piece-wise cubic spline[38] and used to describe the $M_{\text{an}}(H_{\text{eff}})$ relationship in the J-A model. Thus, we consider the technical saturation magnetization M_{s} to be a fixed parameter, and it is implicitly included in the $M_{\text{an}}(H_{\text{eff}})$ magnetization curve. Based on the existing postulates made by Jiles and Atherton[7], we assume that the interaction field αM varies in accordance with the applied field strength. Therefore, the parameter that describes the inter-domain coupling α is assumed to be a non-constant fitting parameter[21] (see (8) and Refs. 25 and 26).

The identified anhysteretic curves for the M400-50A NO silicon steel sheet are shown in Fig. 2. The result shows variations of the anhysteretic magnetization in seven measurement directions. Among the seven measurement directions, the 0° (or the RD) is the magnetically easy direction, whereas 90° (or the TD) is the hard direction. As it appears to be, the $B(H_{\text{avg}})$-characteristics show that the M400-50A possess a significant level of magnetic anisotropy. The level of anisotropy is low for lower values of flux density B, and gradually increases until 1.5 T. At high amplitudes, the domain magnetizations coherently rotate towards the direction of the applied field strength H_{avg}, so the flux density B for all seven different directions converges asymptotically to a single value, so-called the technical saturation magnetization M_{s}[27].

ACCEPTED MANUSCRIPT
AIP Advances
This is the author's peer reviewed, accepted manuscript. However, the online version of record will be different from this version once it has been copyedited and typeset.
PLEASE CITE THIS ARTICLE AS DOI:10.1063/5.0009554
AIP Publishing

D. Description of the J-A model parameters

The interaction between the pinning sites (imperfections, dislocations, and location of inhomogeneous strain) and the domain walls increase with the applied field strength H[7]. As a result, the hysteresis loss dissipation rises. The hysteresis losses depend on the amplitude and direction of the input excitation because the pinning sites are non-uniformly distributed in the material[39]. In addition, the losses also depend on the type of input excitation, unidirectional alternating, and rotational[1,6]. Therefore, the pinning parameter k is not necessarily a constant but a function of the applied field strength H and its alternating direction[40]. In other words, the pinning parameter k, and the parameter describing the reversible wall bending c could be related to the coercive field strength $H_c \approx k(1-c)$[23,41].

It is well observed that the coercive field strength H_c varies as a function of the peak amplitude of applied field strength H[42] (see Fig. 3 in Ref. 42 and Ref. 43). Thus, it can be understood that either k or c varies as a function of the peak amplitude of applied field strength H. Likewise, for an inverse J-A model, the model parameters varies as a function of the peak amplitude of flux density B.

In the literature, several works related to the J-A model are presented, that utilize M (or H)-dependent model parameters. We outline some of the main outcomes from the past works. In Ref. 20, the authors propose to modify the pinning parameter k of the J-A model. In their work, the pinning parameter k is allowed to vary as a function of the bulk magnetization M/M_s and two adjustable coefficients. In Ref. 10, the saturation magnetization M_s, pinning parameter k, and the shape parameters a are identified in nine different directions ($0^\circ - 90^\circ$ every 10° step) of the GO silicon steel sheet sample. As a result, the simulation shows a better fit with the measured unidirectional alternating $B(H)$-characteristics. The J-A model in Ref. 23 is supplied with the variable pinning and reversibility parameters. Both the parameters (k and c) vary as a function of the peak amplitude of the effective field strength H_{eff}. The authors demonstrate that the simulated results with variable pinning and reversibility parameters produce a better fit with the measured $B(H)$-characteristics of a NO silicon steel.

Likewise, the authors in Ref. 43 estimate the pinning, reversible, and the inter-domain coupling parameters of the J-A model for all the measured symmetric minor and major hysteresis loops. Their result shows that the loop-dependent parameters (k, c, and α) produce a better fit with the measured $B(H)$-characteristics in the RD and TD directions. The authors in Ref. 22 express the

ACCEPTED MANUSCRIPT
AIP Advances
This is the author's peer reviewed, accepted manuscript. However, the online version of record will be different from this version once it has been copyedited and typeset.
PLEASE CITE THIS ARTICLE AS DOI:10.1063/5.0009554
AIP Publishing

reversible parameter c as a function of the applied field strength $|H|/H_{\max}$ and two adjustable parameters. In Ref. 44, the pinning parameter k is expressed as a function of the bulk magnetization $|M|/M_{\mathrm{s}}$ and three additional adjustable parameters. Their extended J-A model is then applied to model the $B(H)$-characteristics of $Fe_{40}Ni_{38}Mo_4B_{18}$ amorphous alloy. In Ref. 21, the interaction field αM is extended to higher-order terms. The result shows a better fit with the measured anhysteretic characteristic of polycrystalline iron wire.

Clearly, based on the results from past literature, we can understand that the parameters of the J-A model, specifically k and c, are not constants, which is in line with the postulates made by Jiles and Atherton in Ref. 7. Apart from the M (or H)-amplitude dependence of the model parameters, we find that the directional dependence is somehow not addressed in the past works. Thus, through this work, we try to emphasize that both amplitude, as well as directional dependence of the J-A model parameters are vital from the modeling perspective.

E. Identification of the model parameters

In the past, several techniques are demonstrated for the identification of the parameters of the J-A model[19,45]. The global optimization techniques based on the heuristic methods have become very useful in determining the parameters of the J-A model[46,47]. In this paper, the meta-heuristic Simulated Annealing optimization method is utilized to estimate the model parameters from the measured $B(H)$-characteristics[19]. The algorithm available in Ref. 38 has been fine-tuned for this purpose. The parameters that yield the lowest value of the mean square error between the simulated and measured field strength H has been extracted. Besides, the model parameters are optimized for each of the measured symmetric minor and major hysteresis loops. The identified parameters of the J-A model for seven alternating $B(H)$-characteristics are shown in Fig. 3, Fig. 4, and Fig. 5. The variation in the pinning parameter k w.r.t. the peak amplitude of the applied flux density B is shown in Fig. 3. Similarly, Fig. 4 and Fig. 5 show the variations of the parameters related to the reversible magnetization process, and inter-domain coupling.

The identified parameters (k, α, and c) of the J-A model show specific trend (see Fig. 3, Fig. 4, and Fig. 5). Indeed, they describe the magnetic state of the material. The variation in the pinning and reversible parameters are minimal until 1.3 T and gradually rises until 1.5 T. This typical behavior can be related to the coercive field strength H_{c}, and specifically to the hysteresis losses. The pinning parameters for the high amplitude of flux density B describe the maximum interaction of

ACCEPTED MANUSCRIPT
AIP Advances
This is the author's peer reviewed, accepted manuscript. However, the online version of record will be different from this version once it has been copyedited and typeset.
PLEASE CITE THIS ARTICLE AS DOI:10.1063/5.0009554
AIP Publishing

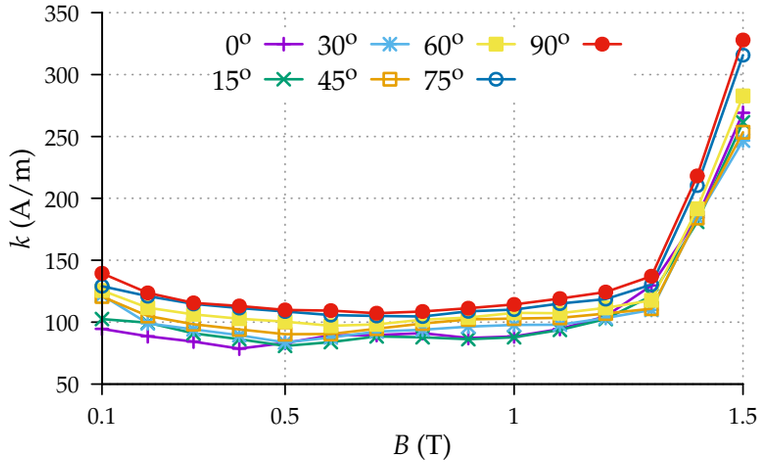

Figure 3: Identified pining parameter k of the J-A model.

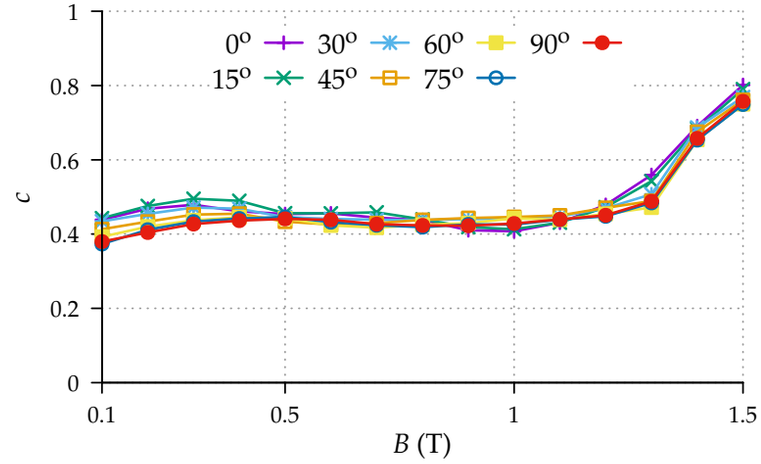

Figure 4: Identified parameter related to the reversible magnetization process c.

the domain walls with the pinning sites. As a result, the coercive field strength H_c attains maximum value. In contrast, the reversibility parameter c at high values of B indicates that the differential susceptibility is asymptotically approaching the value of differential anhysteretic susceptibility. In other words, further changes in the bulk magnetization M is obtained by the coherent rotation of the domain magnetic moments[27].

The inter-domain coupling parameter α shows slightly different behavior (see Fig. 5). According to the result, there seems to be weak coupling between the domain magnetizations at low flux density levels ($B \leq 0.4$ T). For instance, at low values of excitation, the interaction field is negligible. In contrast, at high field excitation, the M400-50A silicon steel is characterized by domains

ACCEPTED MANUSCRIPT
AIP Advances
This is the author's peer reviewed, accepted manuscript. However, the online version of record will be different from this version once it has been copyedited and typeset.
PLEASE CITE THIS ARTICLE AS DOI:10.1063/5.0009554
AIP Publishing

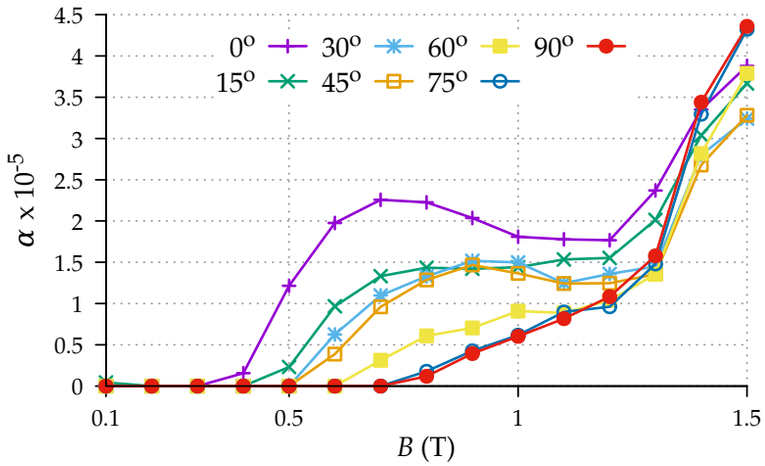

Figure 5: Identified parameter related to the inter-domain coupling α.

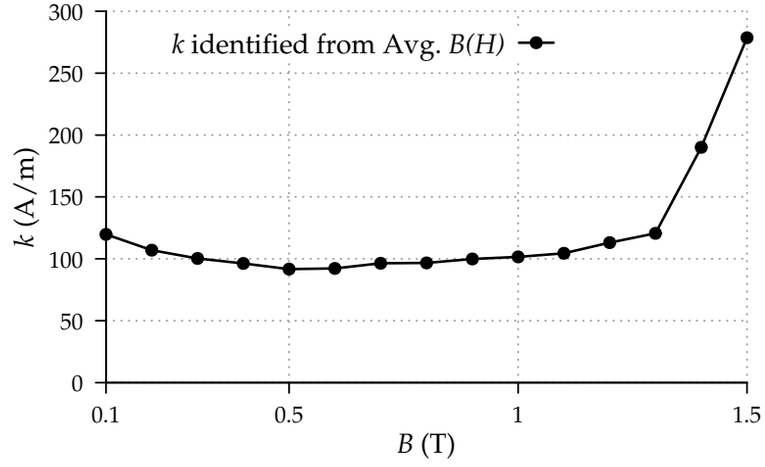

Figure 6: Average values of the pinning parameter k.

having large volumes, which are few in numbers; as a consequence, the interaction between the domains seems to rise. Indeed, at sufficiently high amplitude excitations, a single grain could represent a single domain in a multi-grain sample; therefore, no further increase in interaction is possible[39].

The average values of model parameters, k, α, and c, are shown in Fig. 6, Fig. 7, and Fig. 8. It should be noted that the average values of the model parameters are identified from the averaged $B(H)$-characteristic (see Fig. 1d). The average result could be related to the parameters identified from the $B(H)$-characteristics of the stacked silicon steel sheets, provided that the steel sheets are cut in seven different directions w.r.t. the RD.

ACCEPTED MANUSCRIPT
AIP Advances
This is the author's peer reviewed, accepted manuscript. However, the online version of record will be different from this version once it has been copyedited and typeset.
PLEASE CITE THIS ARTICLE AS DOI:10.1063/5.0009554
AIP Publishing

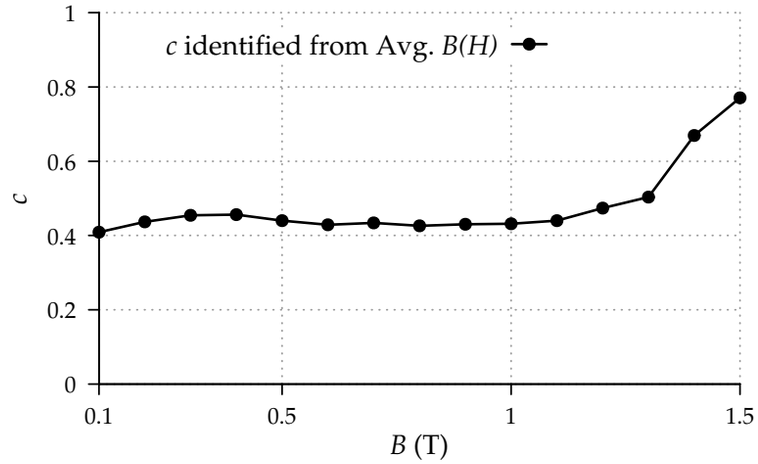

Figure 7: Average values of the parameter related to the reversible magnetization process c.

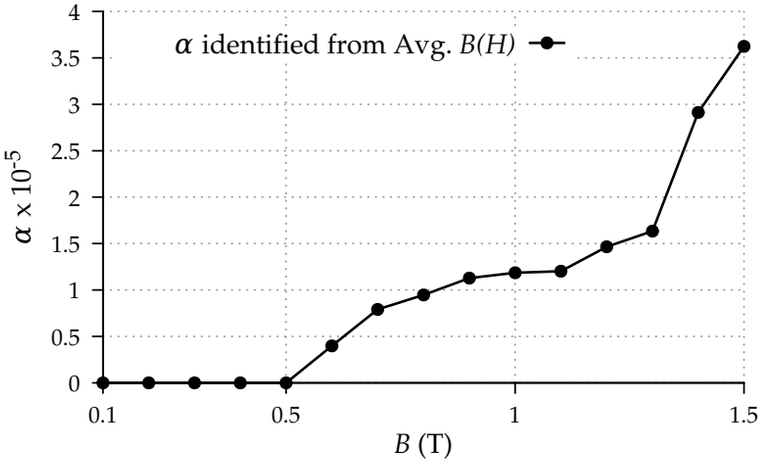

Figure 8: Average values of parameter related to the inter-domain coupling α.

F. Representation of anisotropic parameters

The parameters k, α, and c of the J-A model show smooth variation from the RD to TD (see Fig. 9). The result shows that the parameters depend both on the peak amplitude and direction of the applied flux density B (see Fig. 3, Fig. 4, Fig. 5, and Fig. 9). Therefore, based on the observation, we propose the following model to describe the anisotropic parameters of the J-A model. The parameters are expressed as,

$$k(B,\phi) = \frac{k_{\mathrm{RD}}(B)\,k_{\mathrm{TD}}(B)}{\sqrt{\left(k_{\mathrm{RD}}(B)\sin\phi\right)^2 + \left(k_{\mathrm{TD}}(B)\cos\phi\right)^2}}, \tag{10}$$

ACCEPTED MANUSCRIPT
AIP Advances
This is the author's peer reviewed, accepted manuscript. However, the online version of record will be different from this version once it has been copyedited and typeset.
PLEASE CITE THIS ARTICLE AS DOI:10.1063/5.0009554
AIP Publishing

$$\alpha(B,\phi) = \frac{\alpha_{\mathrm{RD}}(B)\,\alpha_{\mathrm{TD}}(B)}{\sqrt{\left(\alpha_{\mathrm{RD}}(B)\sin\phi\right)^2 + \left(\alpha_{\mathrm{TD}}(B)\cos\phi\right)^2}}, \tag{11}$$

$$c(B,\phi) = \frac{c_{\mathrm{RD}}(B)\,c_{\mathrm{TD}}(B)}{\sqrt{\left(c_{\mathrm{RD}}(B)\sin\phi\right)^2 + \left(c_{\mathrm{TD}}(B)\cos\phi\right)^2}}, \tag{12}$$

where ϕ and B are the direction and amplitude of the flux density vector, and $k_{\mathrm{RD}}(B)$, $\alpha_{\mathrm{RD}}(B)$, and $c_{\mathrm{RD}}(B)$ represent the identified pinning, inter-domain coupling, and reversible parameters based on the $B(H)$-characteristics in the RD. Likewise, $k_{\mathrm{TD}}(B)$, $\alpha_{\mathrm{TD}}(B)$, and $c_{\mathrm{TD}}(B)$ are the model parameters identified in the TD.

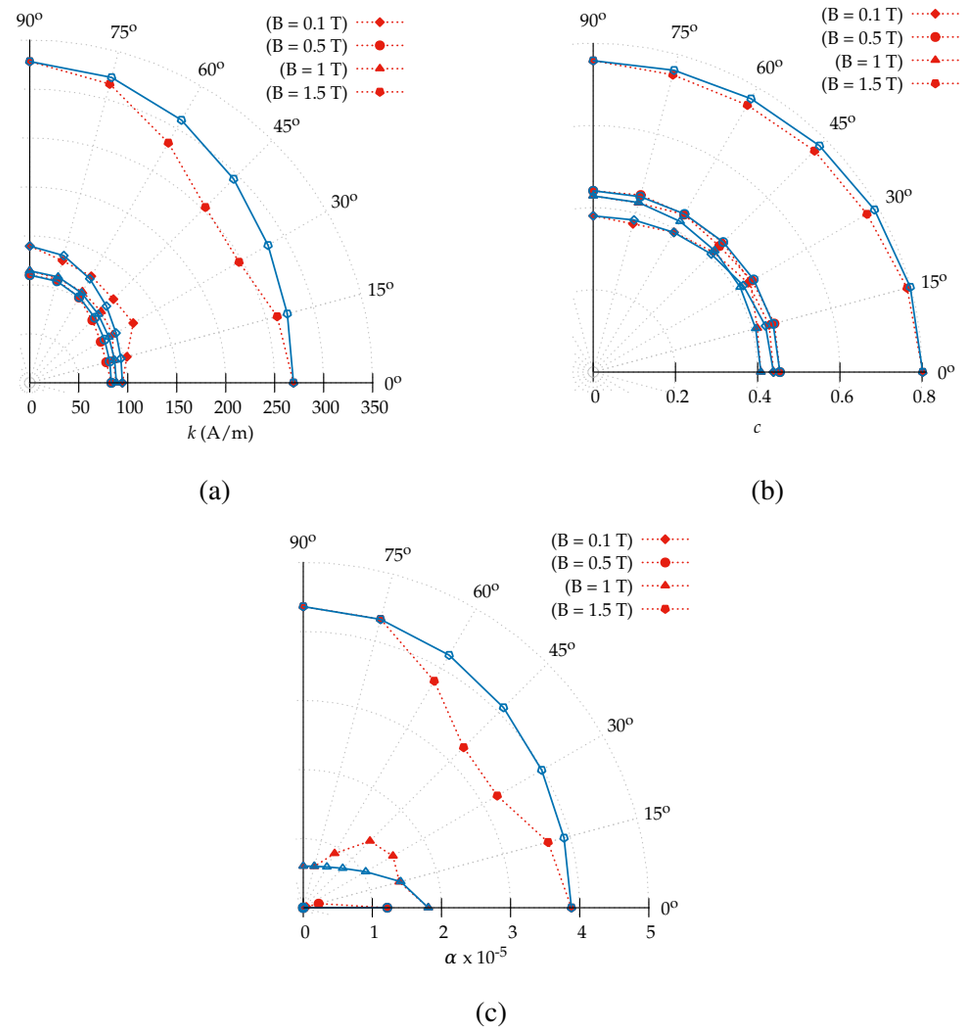

(a) (b)

(c)

Figure 9: Identified (··· dotted), and fitted (— solid) pinning, reversible, and inter-domain coupling parameters of the J-A model. (a) k. (b) c. (c) α.

The following four cases can be considered:

ACCEPTED MANUSCRIPT
AIP Advances
This is the author's peer reviewed, accepted manuscript. However, the online version of record will be different from this version once it has been copyedited and typeset.
PLEASE CITE THIS ARTICLE AS DOI:10.1063/5.0009554
AIP Publishing

(i) $x_{\mathrm{RD}}(B) \neq x_{\mathrm{TD}}(B)$, where $x = \{k, \alpha, c\}$, and $M_{\mathrm{an}} = f(H_{\mathrm{eff}}, \phi)$;

(ii) $x_{\mathrm{RD}}(B) \neq x_{\mathrm{TD}}(B)$, where $x = \{k, \alpha, c\}$, and $M_{\mathrm{an}} = f(H_{\mathrm{eff}})$;

(iii) $x_{\mathrm{RD}}(B) = x_{\mathrm{TD}}(B)$, where $x = \{k, \alpha, c\}$, and $M_{\mathrm{an}} = f(H_{\mathrm{eff}}, \phi)$;

(iv) $x_{\mathrm{RD}}(B) = x_{\mathrm{TD}}(B)$, where $x = \{k, \alpha, c\}$, and $M_{\mathrm{an}} = f(H_{\mathrm{eff}})$.

The first case (i) is the most general case, as it describes the anisotropic J-A model (with anisotropic parameters). The second case, (ii) describes anisotropy in loss dissipation but isotropic anhysteretic magnetization. On the contrary, case (iii) describes isotropic characteristics in loss dissipation and anisotropic anhysteretic magnetization. Accordingly, the case (iv) describes isotropic magnetic characteristics. Based on the results shown in Fig. 2, Fig. 3, Fig. 4, Fig. 5 and Fig. 9, the unidirectional alternating $B(H)$-characteristic observed in M400-50A can be described by the case (i).

The anisotropy introduced by the rolling of the silicon steel result in better anhysteretic characteristics in the RD[42,43] (see Fig. 1 and Fig. 2); therefore, case (ii) may seldom occur in NO silicon steel. Case (iii) is utilized under the application of external stress[18]. It is a common practice to use isotropic J-A model based on case (iv) to model the measured $B(H)$-characteristics obtained from the standard Epstein-frame device and ring core samples[13]. Moreover, case (iv) is preferred in numerical magnetic field computations of rotating electrical machines[48]. The results produced by (10), (11) and (12) are shown in Fig. 9a, Fig. 9b, and Fig. 9c, respectively. It can be observed that for the low and medium amplitude of flux density B, the proposed analytical equations produce a good fit with the identified parameters of the J-A model; however, at high amplitude levels, some discrepancy can be seen.

III. RESULTS

The simulations of the field strength H are performed using isotropic (average parameters) and anisotropic (identified parameters in seven directions, and proposed analytical functions) parameters in the modified J-A model. Fig. 10, Fig. 11, and Fig. 12 show the simulated and measured hysteresis loops for 45° direction w.r.t the RD. It should be noted that the measured hysteresis loops have rotational symmetry w.r.t. the origin, so, only the upper half of the $B(H)$-loop is shown. The result shows that the anisotropic parameters applied to the modified J-A model produce a good fit

ACCEPTED MANUSCRIPT
AIP Advances
This is the author's peer reviewed, accepted manuscript. However, the online version of record will be different from this version once it has been copyedited and typeset.
PLEASE CITE THIS ARTICLE AS DOI:10.1063/5.0009554
AIP Publishing

with the measured data (see Fig. 10 and Fig. 11). In contrast, the J-A model that utilizes average parameters shows a significant level of disagreement with the measurement, particularly for the major $B(H)$-loop. As depicted in Fig. 12c, the simulated $B(H)$-characteristic shows poor fitting for the medium and high amplitude of magnetic-flux density $B > 1.1$ T.

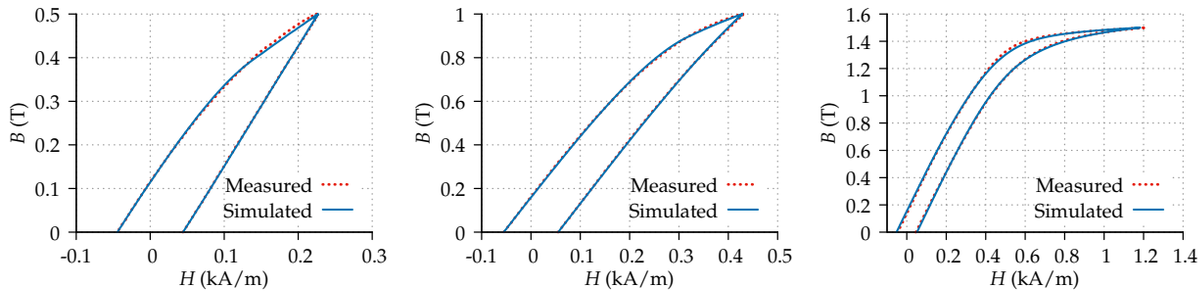

(a) (b) (c)

Figure 10: Simulated and measured $B(H)$-loops for 45° direction w.r.t. the RD. Simulated results are produced using parameters shown in Fig. 2, Fig. 3, Fig. 4, and Fig. 5. (a) $B = 0.5$ T. (b) $B = 1$ T. (c) $B = 1.5$ T.

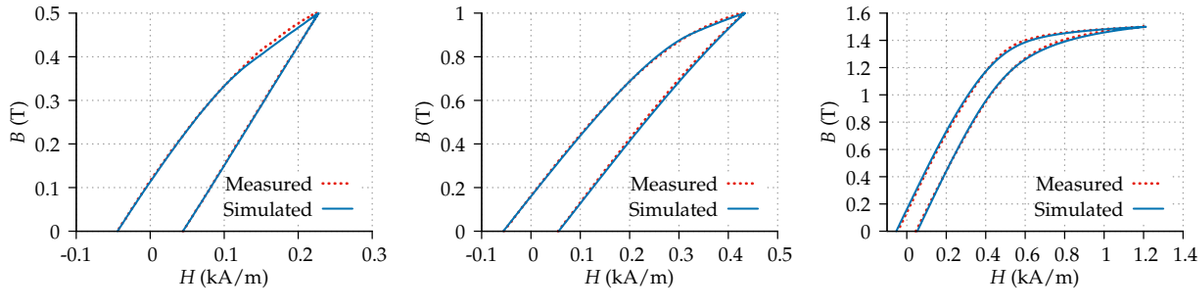

(a) (b) (c)

Figure 11: Simulated and measured $B(H)$-loops for 45° direction. Simulated results are produced using parameters described by the model equations (10), (11), and (12). (a) $B = 0.5$ T. (b) $B = 1$ T. (c) $B = 1.5$ T.

Fig. 13 show the simulated and measured hysteresis losses for seven different directions. Besides, the losses are simulated from six hysteresis loops with peak amplitudes of flux density B being 0.5 T, 0.7 T, 1.0 T, 1.2 T, and 1.5 T. The simulation results shown in Fig. 13a are obtained from the modified J-A model that utilizes anhysteretic magnetization shown in Fig. 2 and the parameters depicted in Fig. 3, Fig. 4 and Fig. 5, respectively. The comparison between the simulated

ACCEPTED MANUSCRIPT
AIP Advances
This is the author's peer reviewed, accepted manuscript. However, the online version of record will be different from this version once it has been copyedited and typeset.
PLEASE CITE THIS ARTICLE AS DOI:10.1063/5.0009554
AIP Publishing

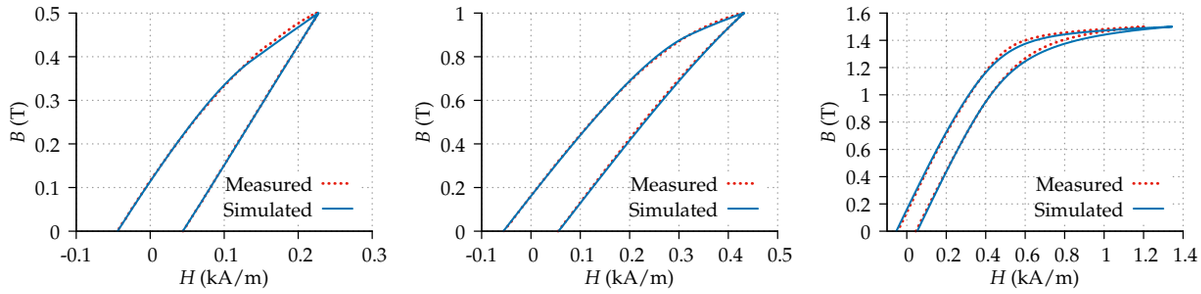

Figure 12: Simulated and measured $B(H)$-loops for 45° direction. Simulated results are produced using parameters shown in Fig. 2, Fig. 6, Fig. 7, and Fig. 8. (a) $B = 0.5$ T. (b) $B = 1$ T. (c) $B = 1.5$ T.

and measured hysteresis losses show that the identified parameters produce sufficiently accurate results (see Fig. 13a). However, at high amplitude excitation ($B = 1.5$ T), the simulated losses are slightly higher than the measured ones.

Fig. 13b shows the losses simulated from the J-A model that uses parameters described by (10), (11), and (12). The result shows a good agreement with the measured losses. In contrast, the J-A model with averaged parameters produces an identical H loci in all seven directions. Therefore, the simulated losses depicted in Fig. 13c are not in good agreement with the measured losses. Besides, it can be observed that the isotropic model overestimates the losses for 0°, 15°, and 30°, whereas it underestimates them for 60°, 75°, and 90°.

IV. CONCLUSION

The pinning, reversible, and the inter-domain coupling parameters of the J-A model depend on the amplitude and direction of the applied magnetic flux density. A suitable analytical function is applied to describe the model parameters (k, α, and c). It is apparent from the simulation results that the model based on the parameters in RD and TD of the NO silicon steel sheet (M400-50A) is sufficient to describe the anisotropic magnetic characteristic in other directions. Apart from the model parameters, the anhysteretic magnetization varies in different measurement directions. The results based on the average (isotropic) parameters of the J-A model show a significant amount of disagreement with the measurement data. Alternatively, the results based on the proposed (modified) J-A model show a good agreement with the measured data.

ACCEPTED MANUSCRIPT
AIP Advances
This is the author's peer reviewed, accepted manuscript. However, the online version of record will be different from this version once it has been copyedited and typeset.
PLEASE CITE THIS ARTICLE AS DOI:10.1063/5.0009554
AIP Publishing

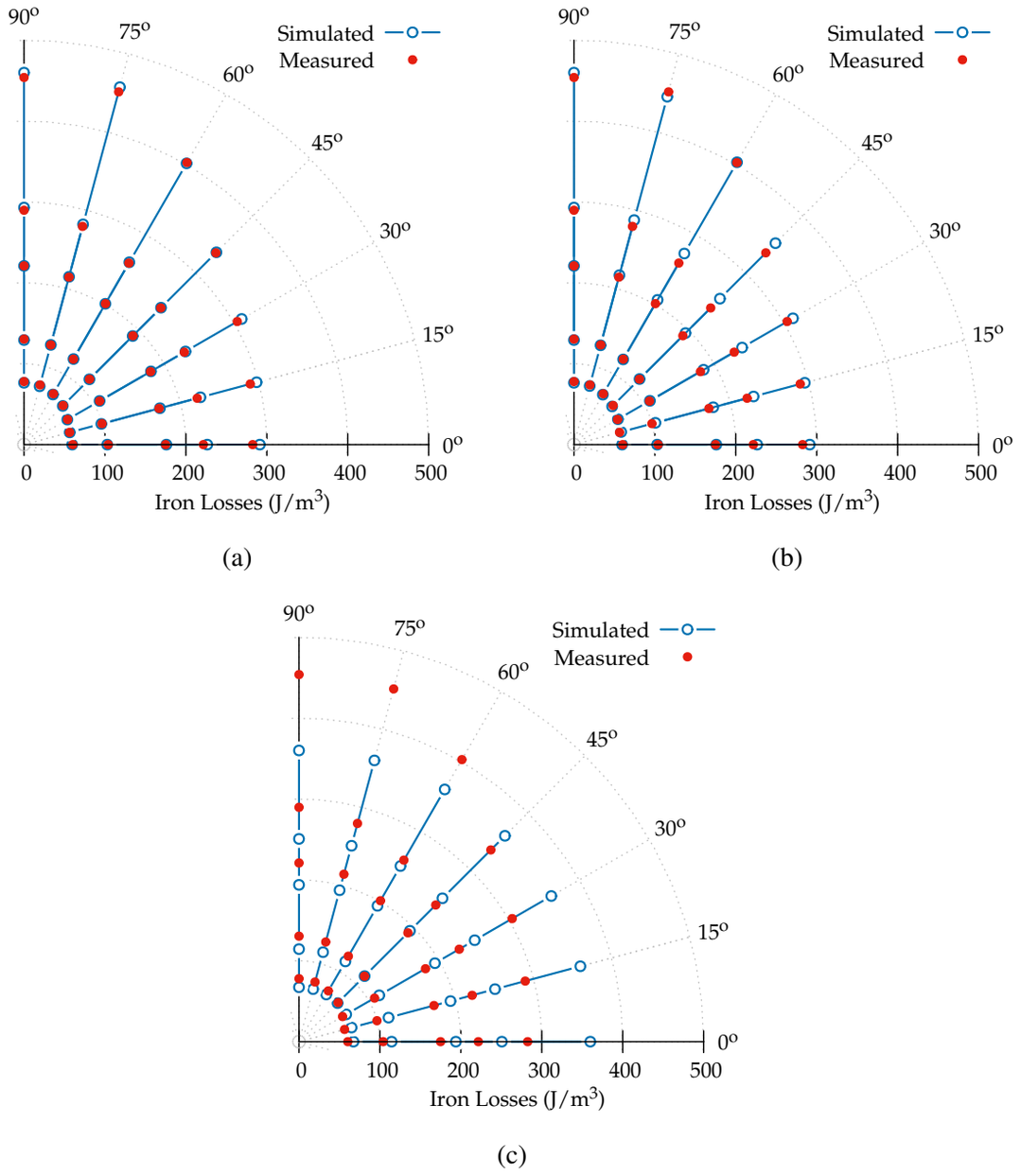

Figure 13: Measured and simulated hysteresis losses in M400-50A, for seven different measurement directions ($B(H)$-loops with peak amplitudes of B being 0.5 T, 0.7 T, 1 T, 1.2 T, and 1.5 T). (a) Simulated results are produced using parameters shown in Fig. 2, Fig. 3, Fig. 4, and Fig. 5. (b) Simulated results are obtained using the proposed model (10), (11), and (12). (c) Simulated results are obtained using the average parameters.

ACCEPTED MANUSCRIPT

AIP Advances

This is the author's peer reviewed, accepted manuscript. However, the online version of record will be different from this version once it has been copyedited and typeset.
PLEASE CITE THIS ARTICLE AS DOI:10.1063/5.0009554

ACKNOWLEDGMENTS

The authors would like to thank the computational resources provided by the Aalto Science-IT Project. This work was supported by the Foundation for Aalto University Science and Technology.

DATA AVAILABILITY STATEMENT

The data that support the findings of this study are available upon reasonable request from the first author. The data are not publicly available.

REFERENCES

[1]N. Nencib, S. Spornic, A. Kedous-Lebouc, and B. Cornut, "Macroscopic anisotropy characterization of SiFe using a rotational single sheet tester," IEEE Trans. Magn. **31**, 4047–4049 (1995).

[2]K. Chwastek, "Anisotropic properties of non-oriented steel sheets," Elec. P. Appl. **7**, 575–579 (2013).

[3]O. Hamrit, O. de la Barrière, M. LoBue, and F. Mazaleyrat, "Anisotropy of losses in non-oriented iron silicon sheets: Influence on electrical machine applications," IEEE Trans. Magn. **52**, 6300107 (2016).

[4]S. Higuchi, T. Nakao, Y. Takahashi, T. Tokumasu, K. Fujiwara, and Y. Ishihara, "Modeling of two-dimensional magnetic properties based on one-dimensional magnetic measurements," IEEE Trans. Magn. **48**, 3486–3489 (2012).

[5]F. J. G. Landgraf, M. Emura, J. C. Teixeira, and M. F. de Campos, "Effect of grain size, deformation, aging and anisotropy on hysteresis loss of electrical steels," J. Magn. Magn. Mater. **215**, 97–99 (2000).

[6]P. Handgruber, A. Stermecki, O. Bíró, V. Goričan, E. Dlala, and G. Ofner, "Anisotropic generalization of vector Preisach hysteresis models for nonoriented steels," IEEE Trans. Magn. **51**, 1–4 (2015).

[7]D. C. Jiles and D. L. Atherton, "Theory of ferromagnetic hysteresis," J. Magn. Magn. Mater. **61**, 48–60 (1986).

[8]D. C. Jiles, J. B. Thoelke, and M. K. Devine, "Numerical determination of hysteresis parameters for the modelling of magnetic properties using the theory of ferromagnetic hysteresis," IEEE Trans. Magn. **28**, 27–35 (1992).

AIP Publishing

ACCEPTED MANUSCRIPT
AIP Advances
This is the author's peer reviewed, accepted manuscript. However, the online version of record will be different from this version once it has been copyedited and typeset.
PLEASE CITE THIS ARTICLE AS DOI:10.1063/5.0009554
AIP Publishing

[9]A. Ramesh, D. C. Jiles, and J. M. Roderick, "A model of anisotropic anhysteretic magnetization," IEEE Trans. Magn. **32**, 4234–4236 (1996).

[10]A. P. S. Baghel, B. S. Ram, K. Chwastek, L. Daniel, and S. V. Kulkarni, "Hysteresis modelling of the GO laminations for arbitrary in-plane directions taking into account the dynamics of orthogonal domain walls," J. Magn. Magn. Mater. **418**, 14–20 (2016).

[11]I. D. Mayergoyz, *Mathematical Models of Hysteresis and Their Applications* (Elsevier Science, New York, 2003).

[12]F. Henrotte and K. Hameyer, "A dynamical vector hysteresis model based on an energy approach," IEEE Trans. Magn. **42**, 899–902 (2006).

[13]A. Benabou, S. Clénet, and F. Piriou, "Comparison of Preisach and Jiles-Atherton models to take into account hysteresis phenomenon for finite element analysis," J. Magn. Magn. Mater. **261**, 139–160 (2003).

[14]A. Bergqvist, "A simple vector generalization of the Jiles-Atherton model of hysteresis," IEEE Trans. Magn. **32**, 4213–4215 (1996).

[15]J. V. Leite, M. V. F. da Luz, N. Sadowski, and P. A. da Silva Jr., "Modelling dynamic losses under rotational magnetic flux," IEEE Trans. Magn. **48**, 895–898 (2012).

[16]B. Upadhaya, F. Martin, P. Rasilo, P. Handgruber, A. Belahcen, and A. Arkkio, "Modelling anisotropy in non-oriented electrical steel sheet using vector Jiles-Atherton model," COMPEL **36**, 764–773 (2017).

[17]P. Andrei, O. Caltun, and A. Stancu, "Differential phenomenological models for the magnetization processes in soft MnZn ferrites," IEEE Trans. Magn. **34**, 231–241 (1998).

[18]M. J. Sablik and D. C. Jiles, "Coupled magnetoelastic theory of magnetic and magnetostrictive hysteresis," IEEE Trans. Magn. **29**, 2113–2123 (1993).

[19]D. Lederer, H. Igarashi, A. Kost, and T. Honma, "On the parameter identification and application of the Jiles-Atherton hysteresis model for numerical modeling of measured characteristics," IEEE Trans. Magn. **35**, 1211–1214 (1999).

[20]Z. Włodarski and J. Włodarska, "Evaluation of hysteresis loss using variable pinning parameter," COMPEL **22**, 328–336 (2001).

[21]B. Kvasnica and F. Kundracík, "Fitting experimental anhysteretic curves of ferromagnetic materials and investigation of the effect of temperature and tensile stress," J. Magn. Magn. Mater. **162**, 43–49 (1996).

ACCEPTED MANUSCRIPT
AIP Advances
This is the author's peer reviewed, accepted manuscript. However, the online version of record will be different from this version once it has been copyedited and typeset.
PLEASE CITE THIS ARTICLE AS DOI:10.1063/5.0009554
AIP Publishing

[22]D. Miljavec and B. Zidarič, "Introducing a domain flexing function in the Jiles-Atherton hysteresis model," J. Magn. Magn. Mater. **320**, 763–768 (2008).

[23]Z. Gmyrek, "Numerical modeling of static hysteresis loop using variable parameters," Int. J. Numer. Model. **27**, 199–212 (2014).

[24]K. Chwastek, J. SzczygŁowski, and W. Wilczyński, "Modelling magnetic properties of high silicon steel," J. Magn. Magn. Mater. **322**, 799–803 (2010).

[25]J. V. Leite, N. Sadowski, P. Kuo-Peng, N. J. Batistela, J. P. A. Bastos, and A. A. de Espíndola, "Inverse Jiles-Atherton vector hysteresis model," IEEE Trans. Magn. **40**, 1769–1775 (2004).

[26]N. Sadowski, N. J. Batistela, J. P. A. Bastos, and M. Lajoie-Mazenc, "An inverse Jiles-Atherton model to take into account hysteresis in time-stepping finite-element calculations," IEEE Trans. Magn. **38**, 797–800 (2002).

[27]B. D. Cullity and C. D. Graham, *Introduction to Magnetic Materials*, 2nd ed. (Wiley, New Jersey, 2009).

[28]M. Abramowitz and I. A. Stegun, *Handbook of Mathematical Functions with Formulas, Graphs, and Mathematical Tables*, 10th ed. (Dover, New York, 1972) Chap. 25.

[29]V. Goričan, A. Hamler, B. Hribernik, M. Jesenik, and M. Trlep, "Proceedings of 6th international workshop on 1&2-dimensional magnetic measurement and testing," (Bad Gastein, Austria, 2000) pp. 66–75.

[30]A. Ramesh, D. C. Jiles, and Y. Bi, "Generalization of hysteresis modeling to anisotropic materials," J. Appl. Phys. **81**, 5585–5587 (1997).

[31]A. Raghunathan, Y. Melikhov, J. E. Snyder, and D. C. Jiles, "Generalized form of anhysteretic magnetization function for Jiles-Atherton theory of hysteresis," Appl. Phys. Letters **95**, 172510 (2009).

[32]A. Iványi, *Hysteresis models in electromagnetic computation* (Akadémiai Kiadó, Budapest, 1997).

[33]E. Kokornaczyk and M. W. Gutowski, "Anhysteretic functions for the Jiles-Atherton model," IEEE Trans. Magn. **51**, 1–5 (2015).

[34]S. Steentjes, M. Petrun, G. Glehn, D. Dolinar, and K. Hameyer, "Suitability of the double langevin function for description of anhysteretic magnetization curves in NO and GO electrical steel grades," AIP Advances **7**, 056013 (2017).

[35]L. Daniel, O. Hubert, N. Buiron, and R. Billardon, "Reversible magneto-elastic behavior: A multiscale approach," J. Mech. Phys. Solids **56**, 1018–1042 (2008).

ACCEPTED MANUSCRIPT
AIP Advances
This is the author's peer reviewed, accepted manuscript. However, the online version of record will be different from this version once it has been copyedited and typeset.
PLEASE CITE THIS ARTICLE AS DOI:10.1063/5.0009554
AIP Publishing

[36]J. H. Krah and A. J. Bergqvist, "Numerical optimization of a hysteresis model," Physica B: Condens. Matter **343**, 35–38 (2004).

[37]S. E. Zirka, Y. I. Moroz, R. G. Harrison, and K. Chwastek, "On physical aspects of the Jiles-Atherton hysteresis models," J. Appl. Phys. **112**, 043916 (2012).

[38]M. Galassi *et al.*, *GNU Scientific Library Reference Manual*, GNU, http://www.gnu.org/software/gsl/, 3rd ed.

[39]A. Hubert and R. Schäfer, *Magnetic Domains: The Analysis of Magnetic Microstructures* (Springer, Berlin, 1998).

[40]Z. Włodarski, "The Jiles-Atherton model with variable pinning parameter," IEEE Trans. Magn. **39**, 1990–1992 (2003).

[41]H. Hauser, Y. Melikhov, and D. C. Jiles, "Examination of the equivalence of ferromagnetic hysteresis models describing the dependence of magnetization on magnetic field and stress," IEEE Trans. Magn. **45**, 1940–1949 (2009).

[42]K. Jacques, S. Steentjes, F. Henrotte, C. Geuzaine, and K. Hameyer, "Representation of microstructural features and magnetic anisotropy of electrical steels in an energy-based vector hysteresis model," AIP Advances **8**, 047602 (2018).

[43]B. Upadhaya, P. Rasilo, L. Perkkiö, P. Handgruber, A. Belahcen, and A. Arkkio, "Comparison of anisotropic Energy-based and Jiles-Atherton models of ferromagnetic hysteresis," IEEE Trans. Magn. **56**, 1–7 (2020).

[44]R. Szewczyk, "Extension of the model of the magnetic characteristics of anisotropic metallic glasses," J. Phys. D: Appl. Phys. **40**, 4109–4113 (2007).

[45]F. R. Fulginei and A. Salvini, "Softcomputing for the identification of the Jiles-Atherton model parameters," IEEE Trans. Magn. **41**, 1100–1108 (2005).

[46]P. R. Wilson, J. N. Ross, and A. D. Brown, "Optimizing the Jiles-Atherton model of hysteresis by a genetic algorithm," IEEE Trans. Magn. **37**, 1211–1214 (2001).

[47]R. Marion, R. Scorretti, N. Siauve, M.-A. Raulet, and L. Krähenbühl, "Identification of Jiles-Atherton model parameters using particle swarm optimization," IEEE Trans. Magn. **44**, 894–897 (2008).

[48]J. B. Padilha, P. Kuo-Peng, N. Sadowski, and N. J. Batistela, "Vector hysteresis model associated with FEM in a self-excited induction generator modeling," IEEE Trans. Magn. **52**, 7000304 (2016).

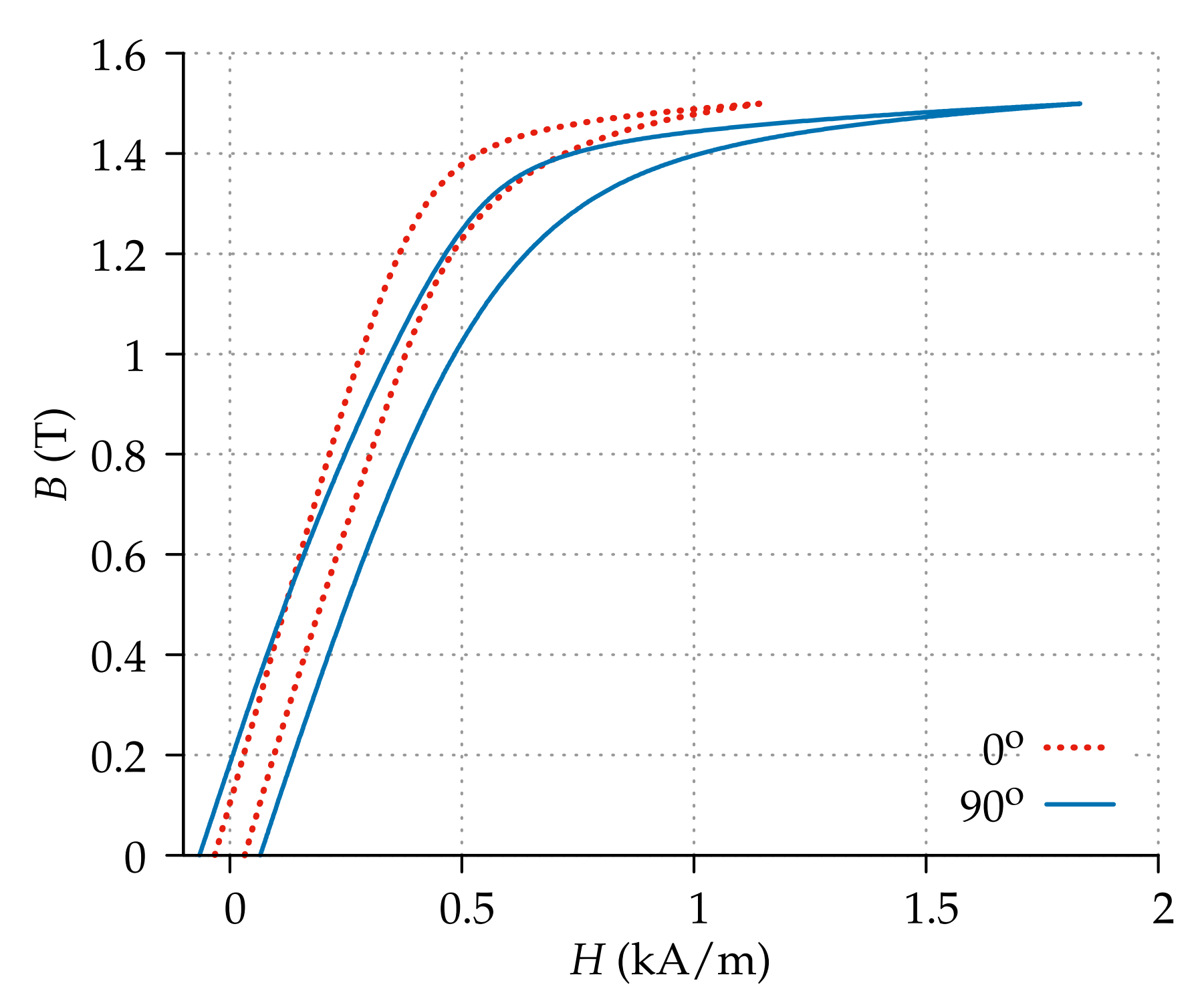
1.6
1.4
1.2
1
0.8
0.6
0.4
0.2
0
B (T)
0
0.5
1
1.5
2
H (kA/m)
0°
90°

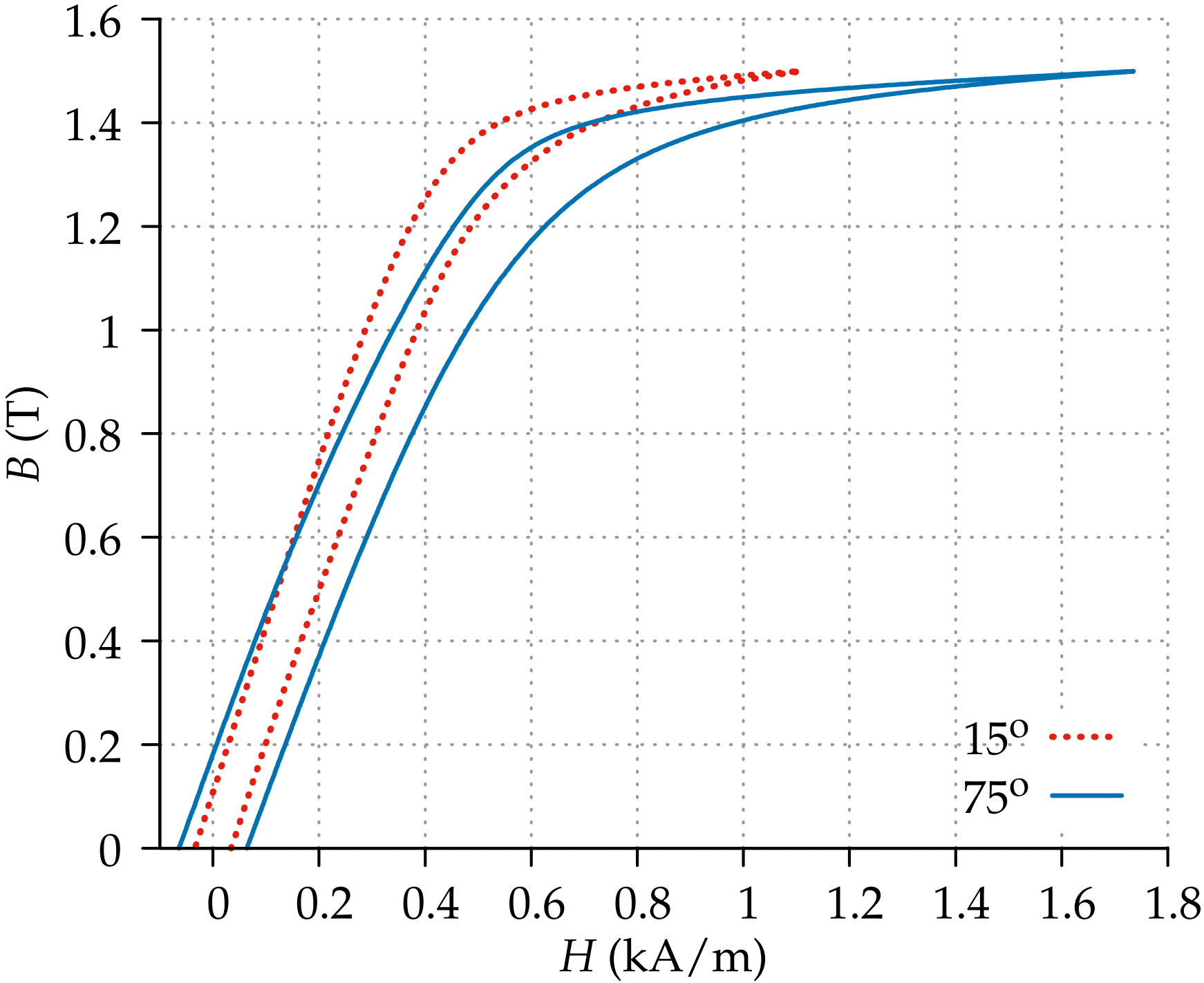
1.6
1.4
1.2
1
0.8
0.6
0.4
0.2
0
B (T)
0
0.2
0.4
0.6
0.8
1
1.2
1.4
1.6
1.8
H (kA/m)
15°
75°

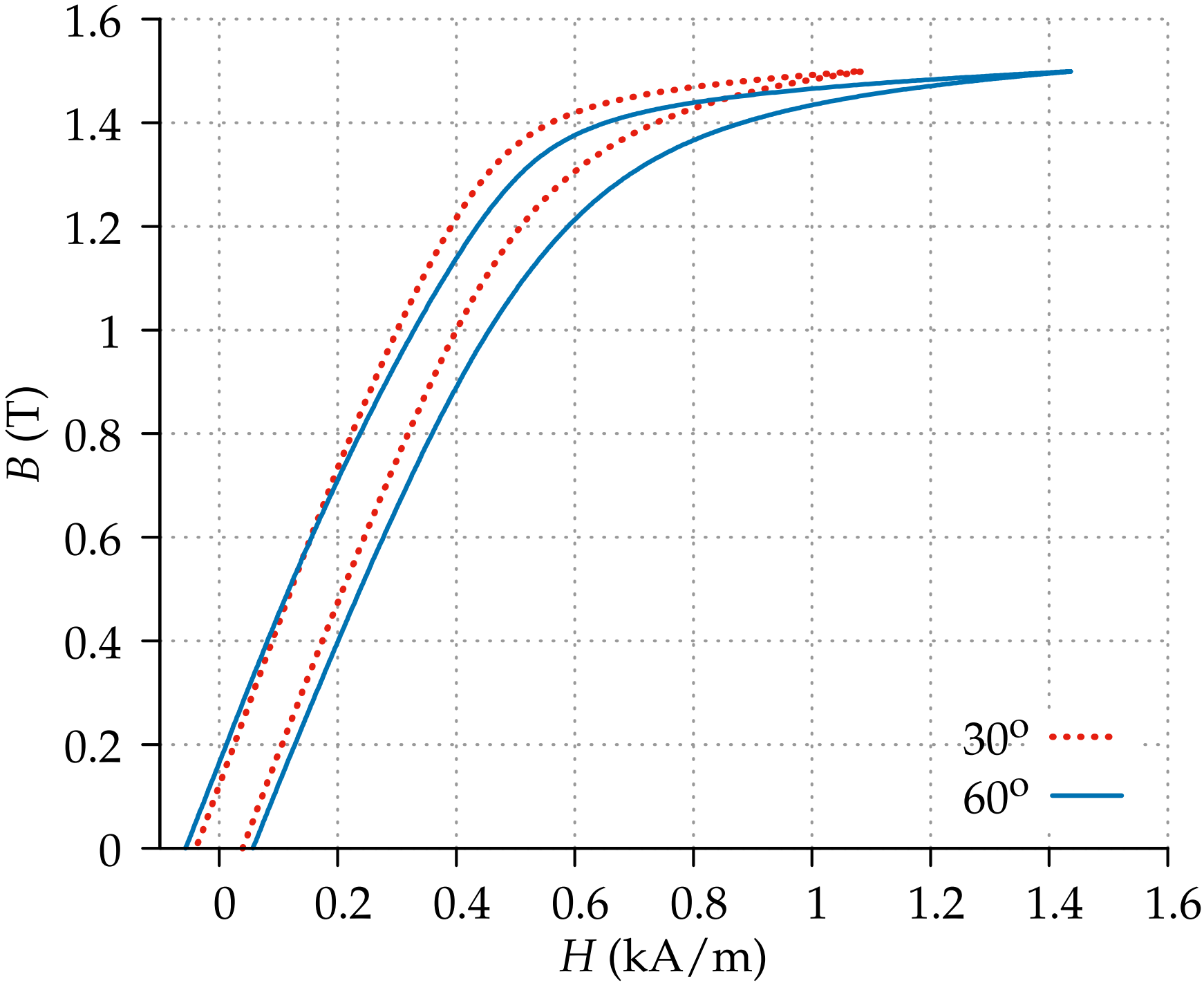
1.6
1.4
1.2
1
0.8
0.6
0.4
0.2
0
B (T)
0
0.2
0.4
0.6
0.8
1
1.2
1.4
1.6
H (kA/m)
30°
60°

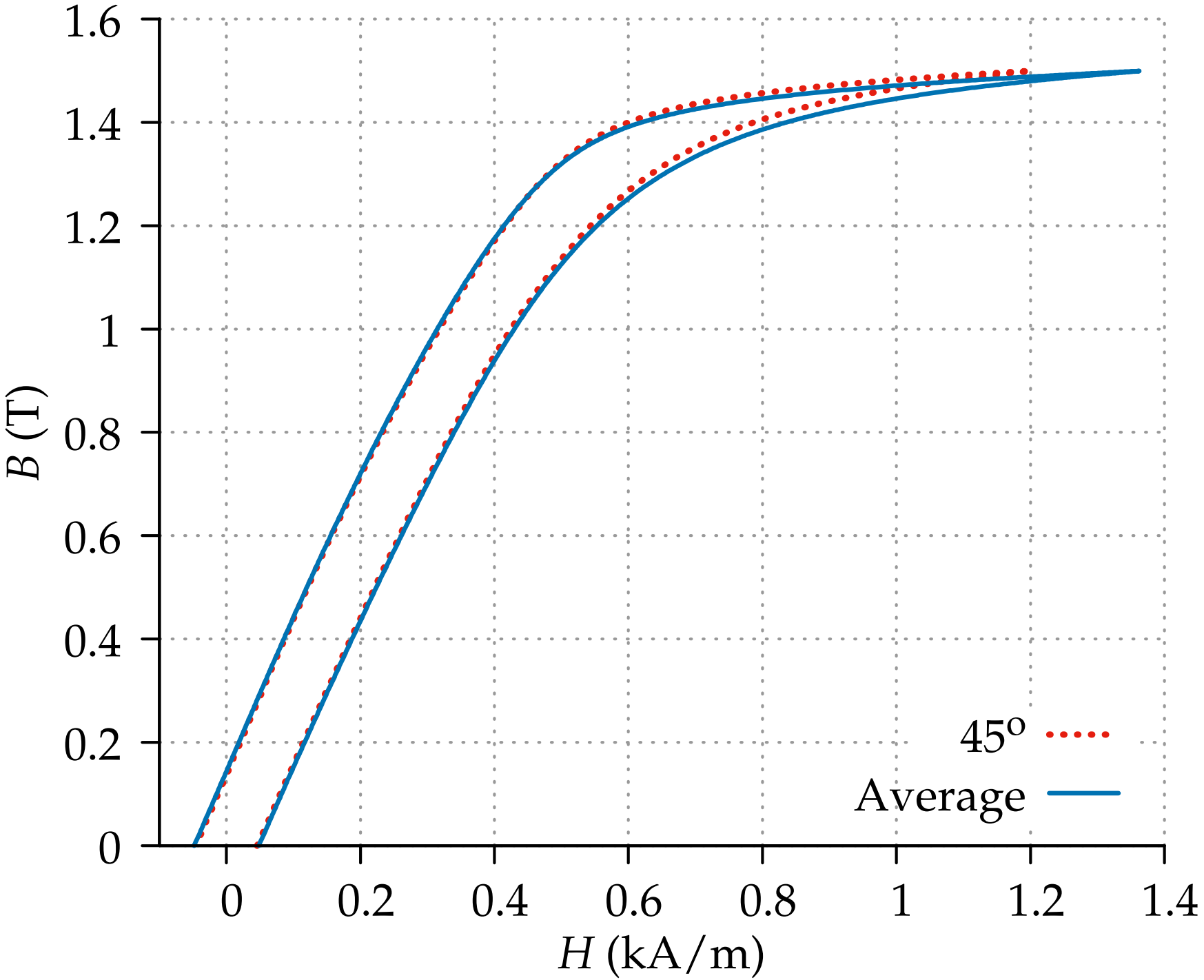
1.6
1.4
1.2
1
0.8
0.6
0.4
0.2
0
B (T)
0
0.2
0.4
0.6
0.8
1
1.2
1.4
H (kA/m)
45°
Average

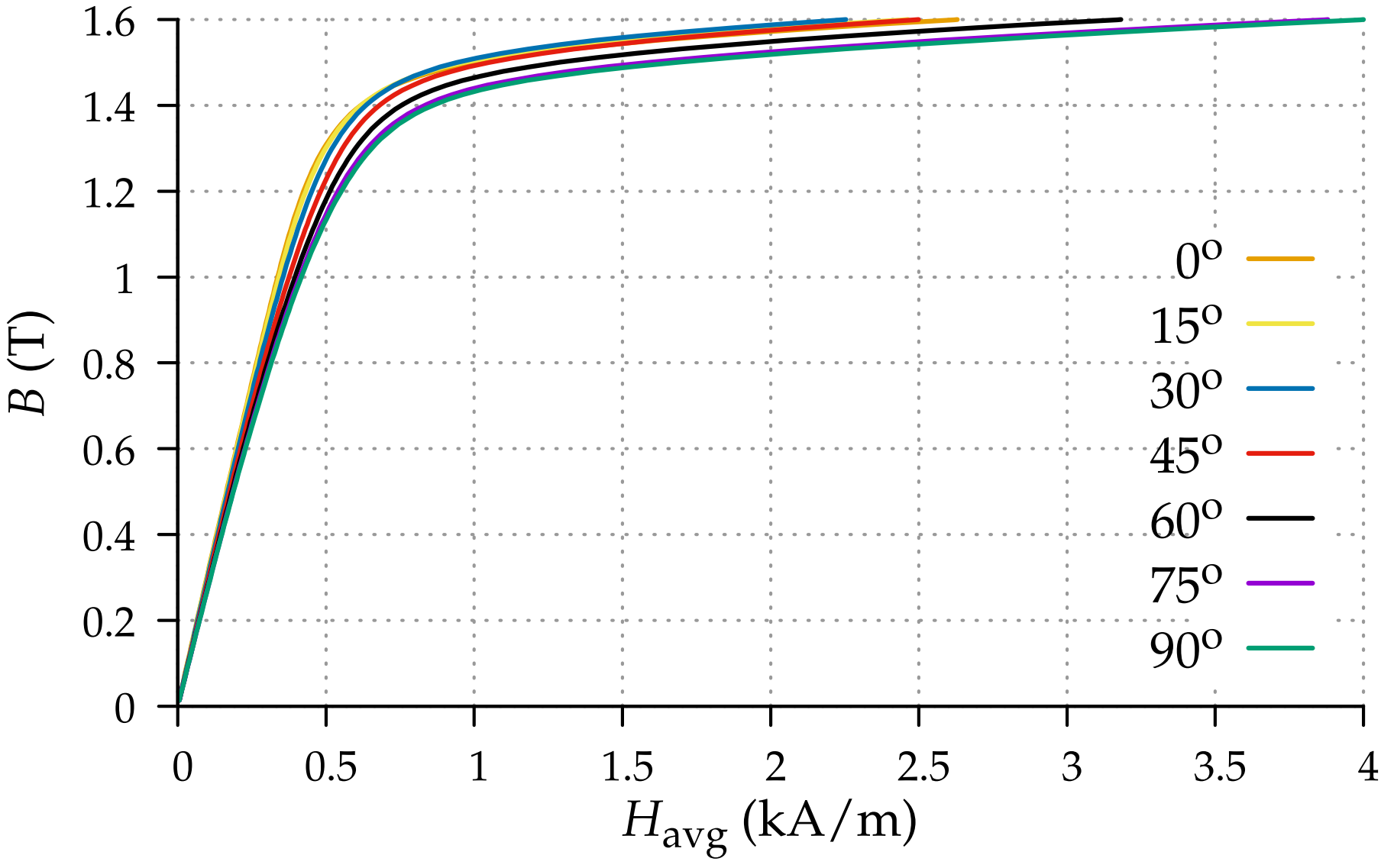
1.6
1.4
1.2
1
0.8
0.6
0.4
0.2
0
B (T)
0
0.5
1
1.5
2
2.5
3
3.5
4
H_avg (kA/m)
0°
15°
30°
45°
60°
75°
90°

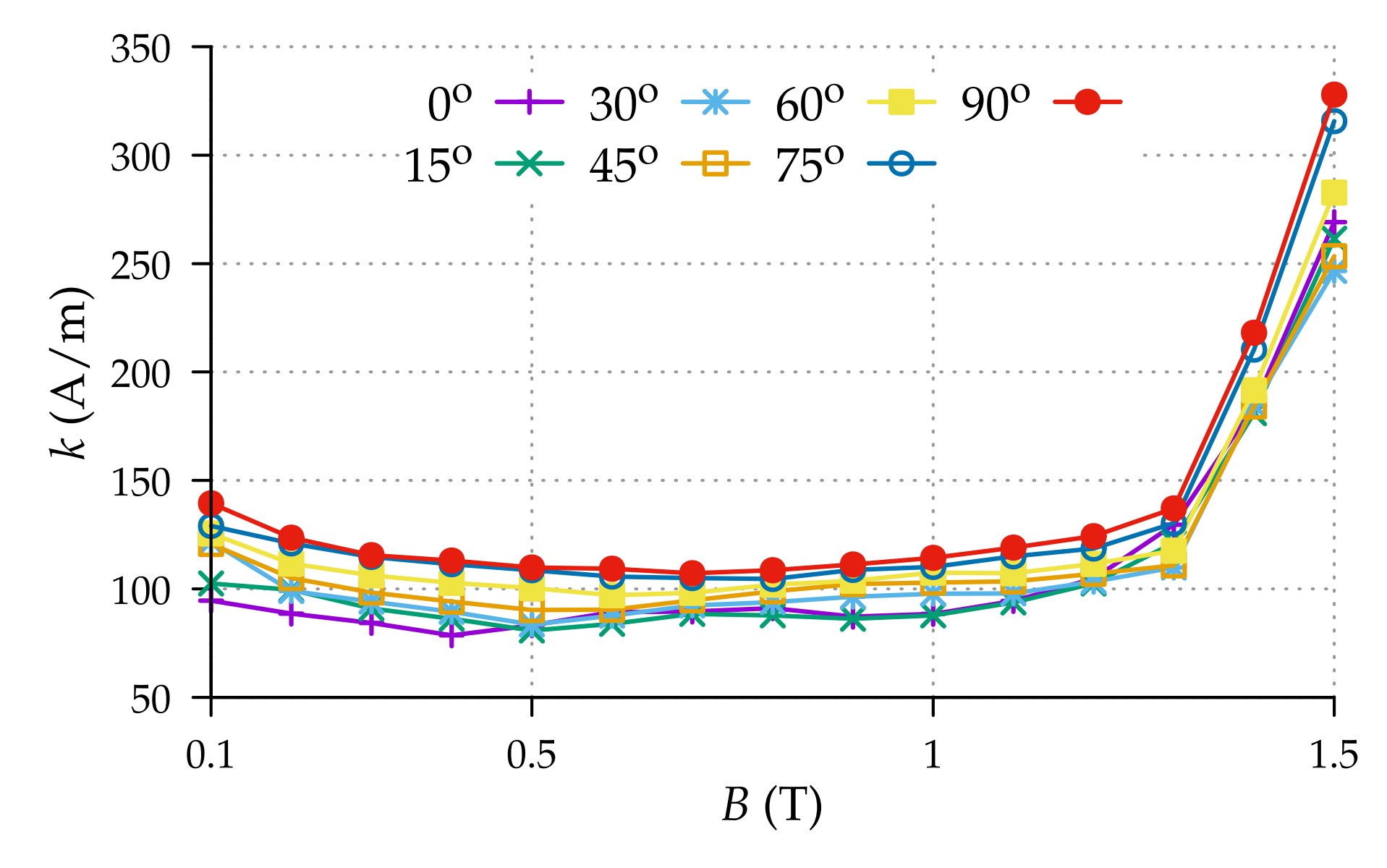
0°
15°
30°
45°
60°
75°
90°
350
300
250
200
150
100
50
k (A/m)
0.1
0.5
1
1.5
B (T)

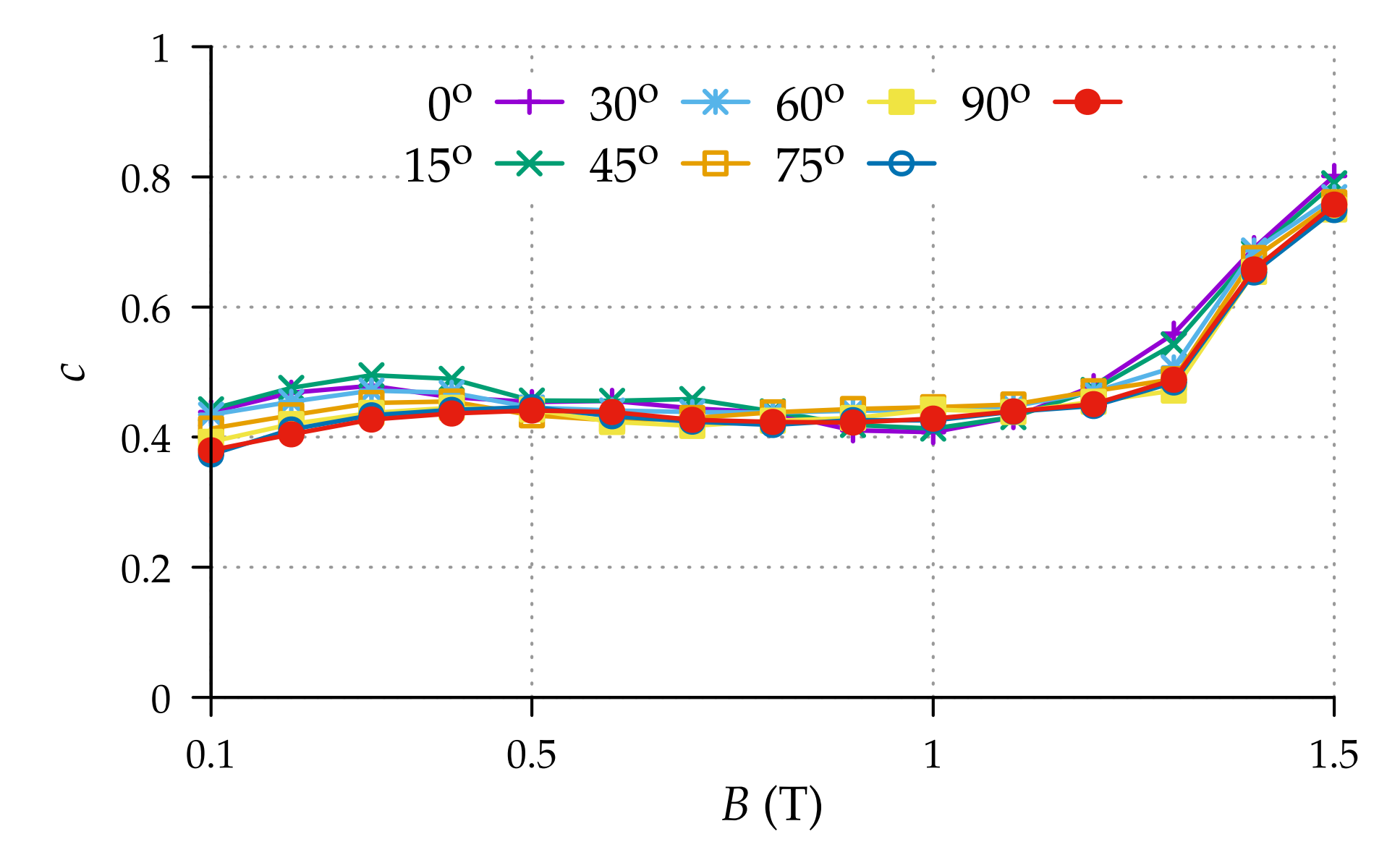
0°
30°
60°
90°
15°
45°
75°
1
0.8
0.6
0.4
0.2
0
c
0.1
0.5
1
1.5
B (T)

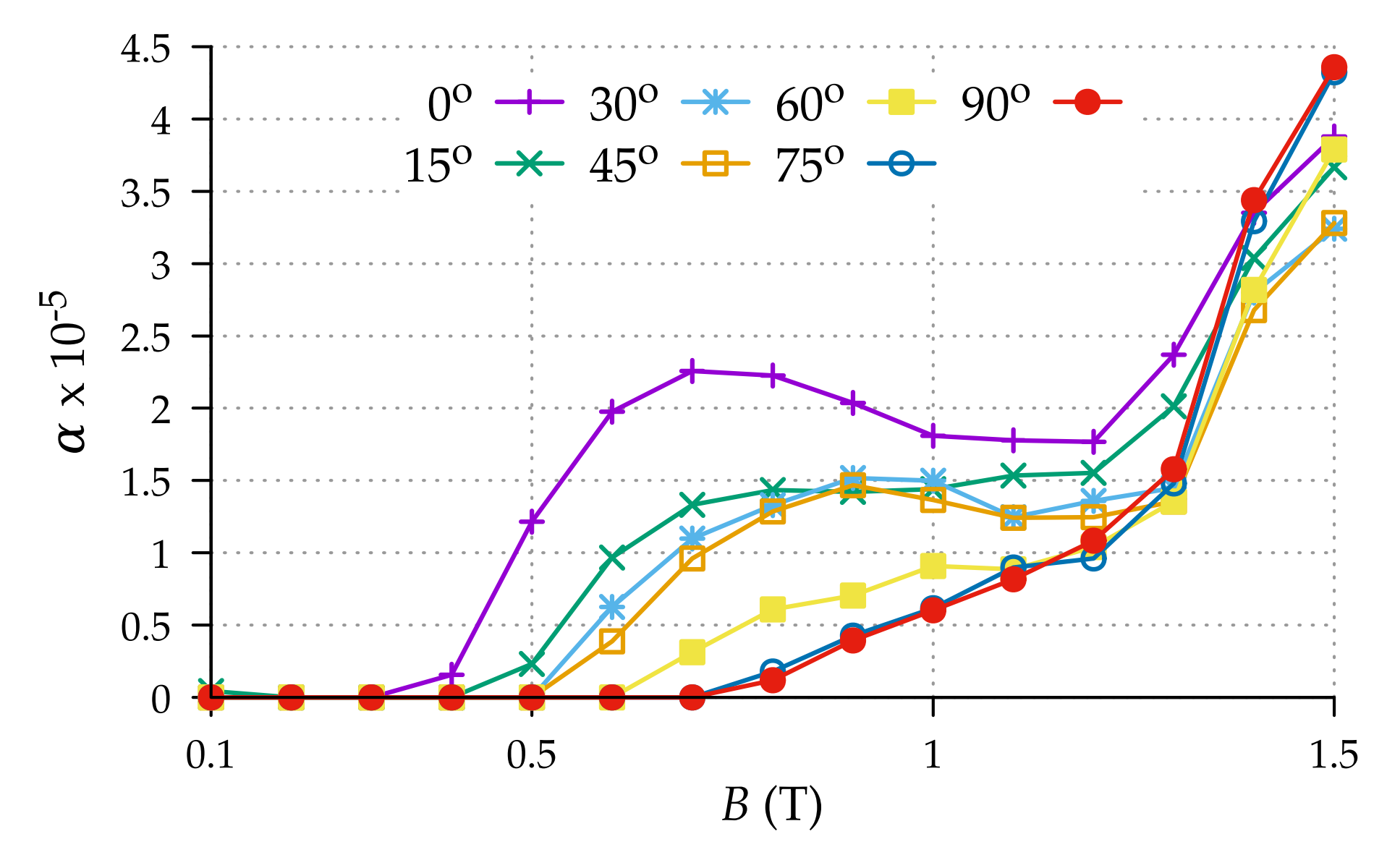
0°
30°
60°
90°
15°
45°
75°
4.5
4
3.5
3
2.5
2
1.5
1
0.5
0
α x 10-5
0.1
0.5
1
1.5
B (T)

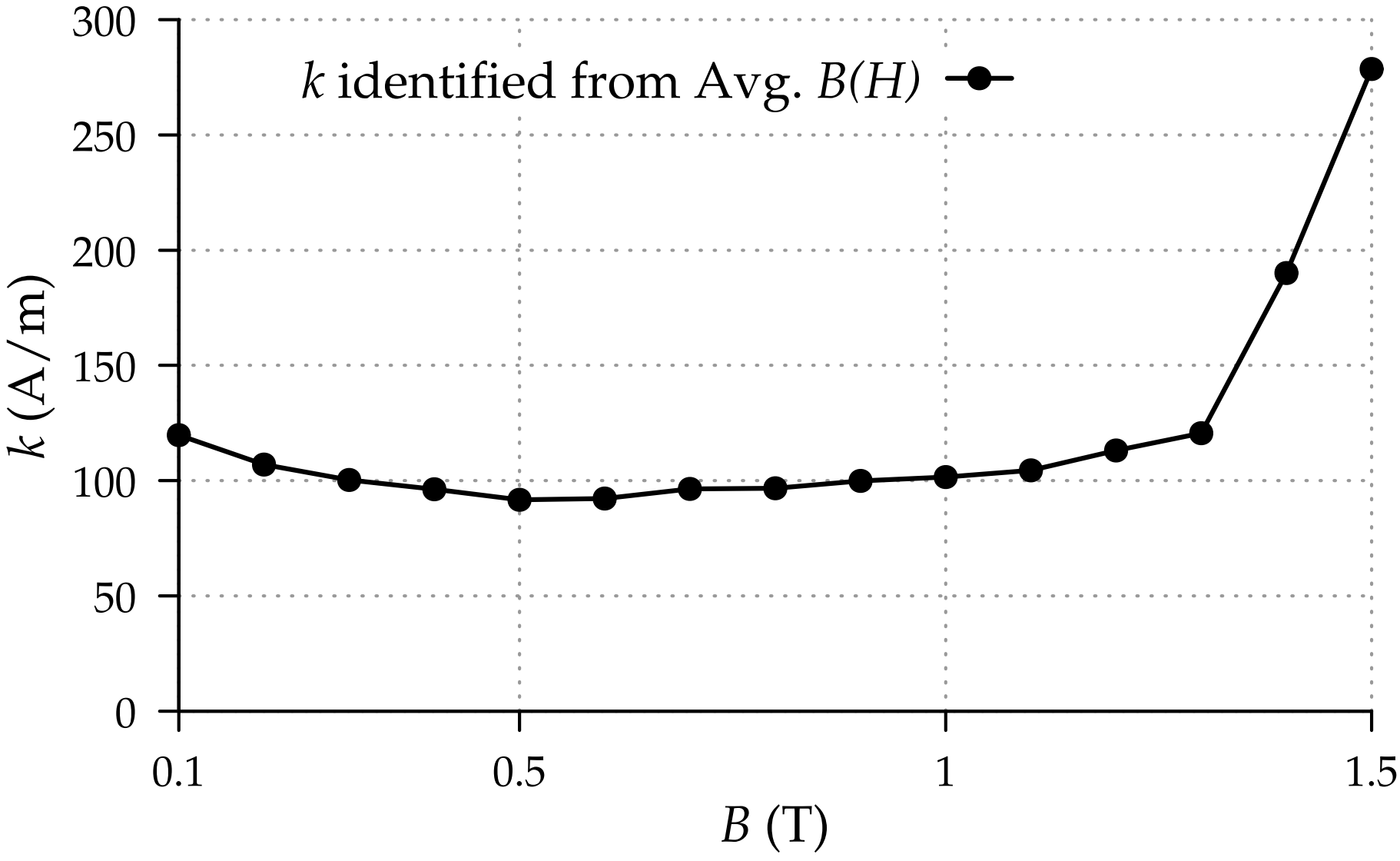
300
250
200
150
100
50
0
k (A/m)
k identified from Avg. B(H)
0.1
0.5
1
1.5
B (T)

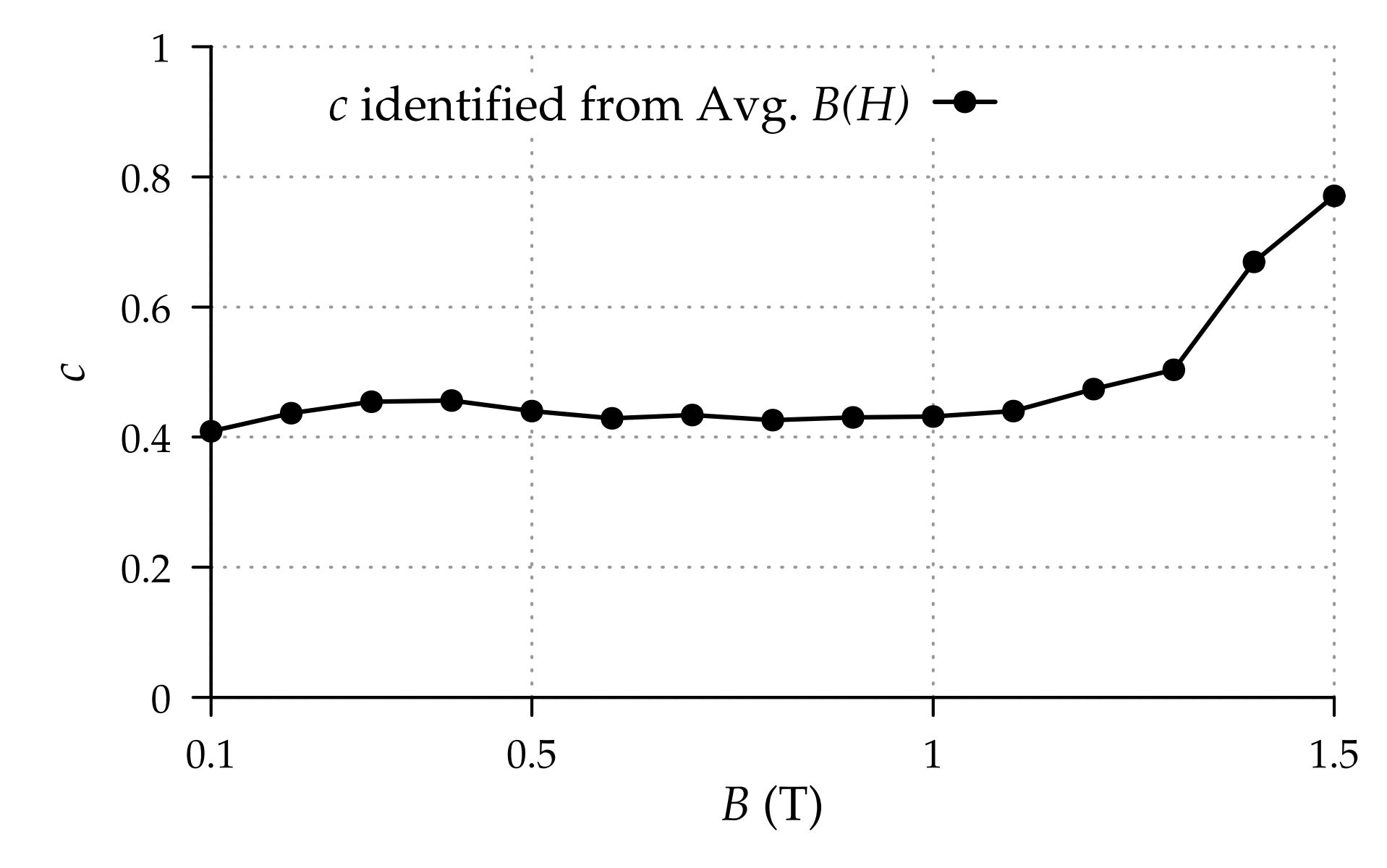
c identified from Avg. B(H)
1
0.8
0.6
0.4
0.2
0
c
0.1
0.5
1
1.5
B (T)

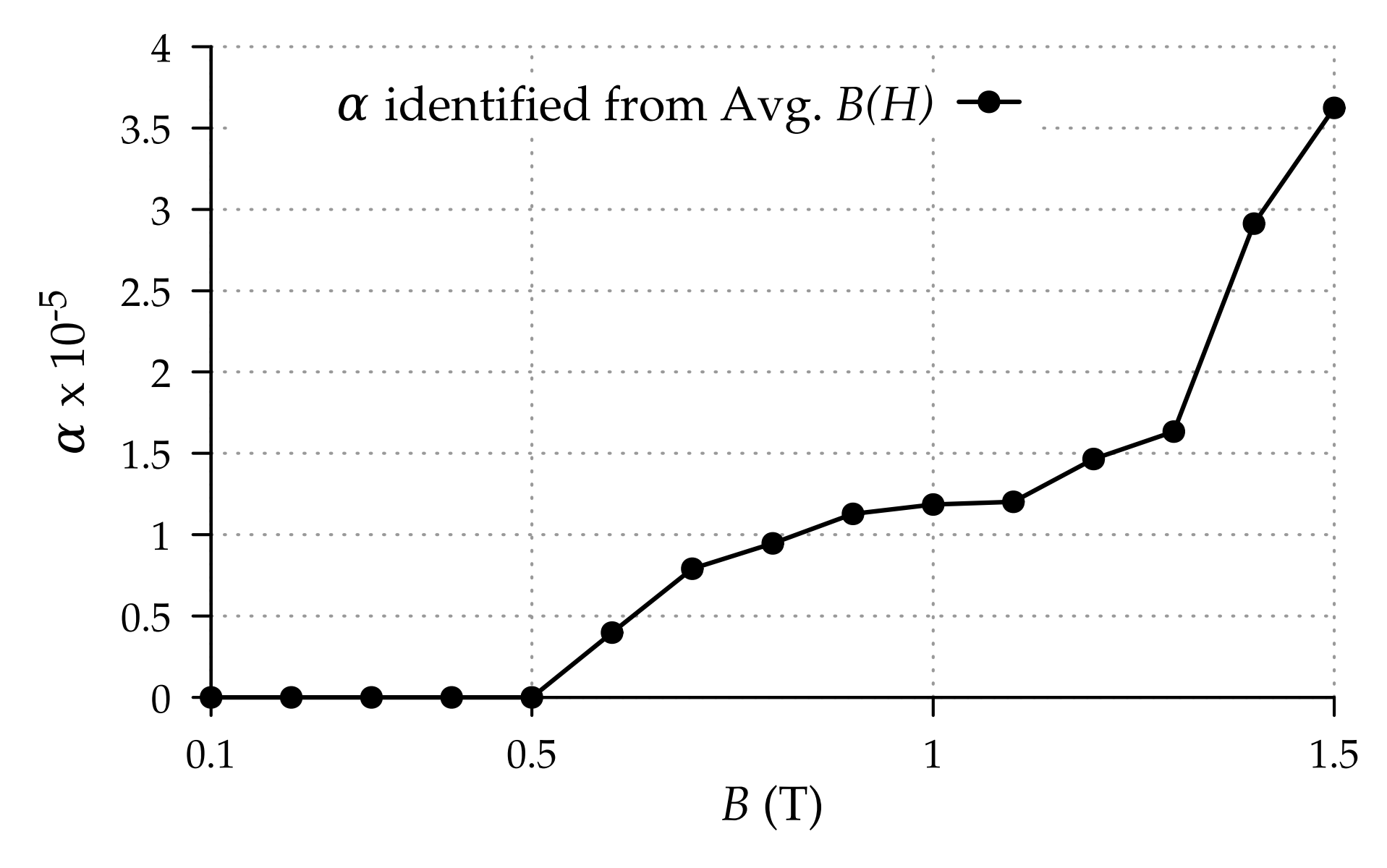
α identified from Avg. B(H)
α x 10-5
4
3.5
3
2.5
2
1.5
1
0.5
0
0.1
0.5
1
1.5
B (T)

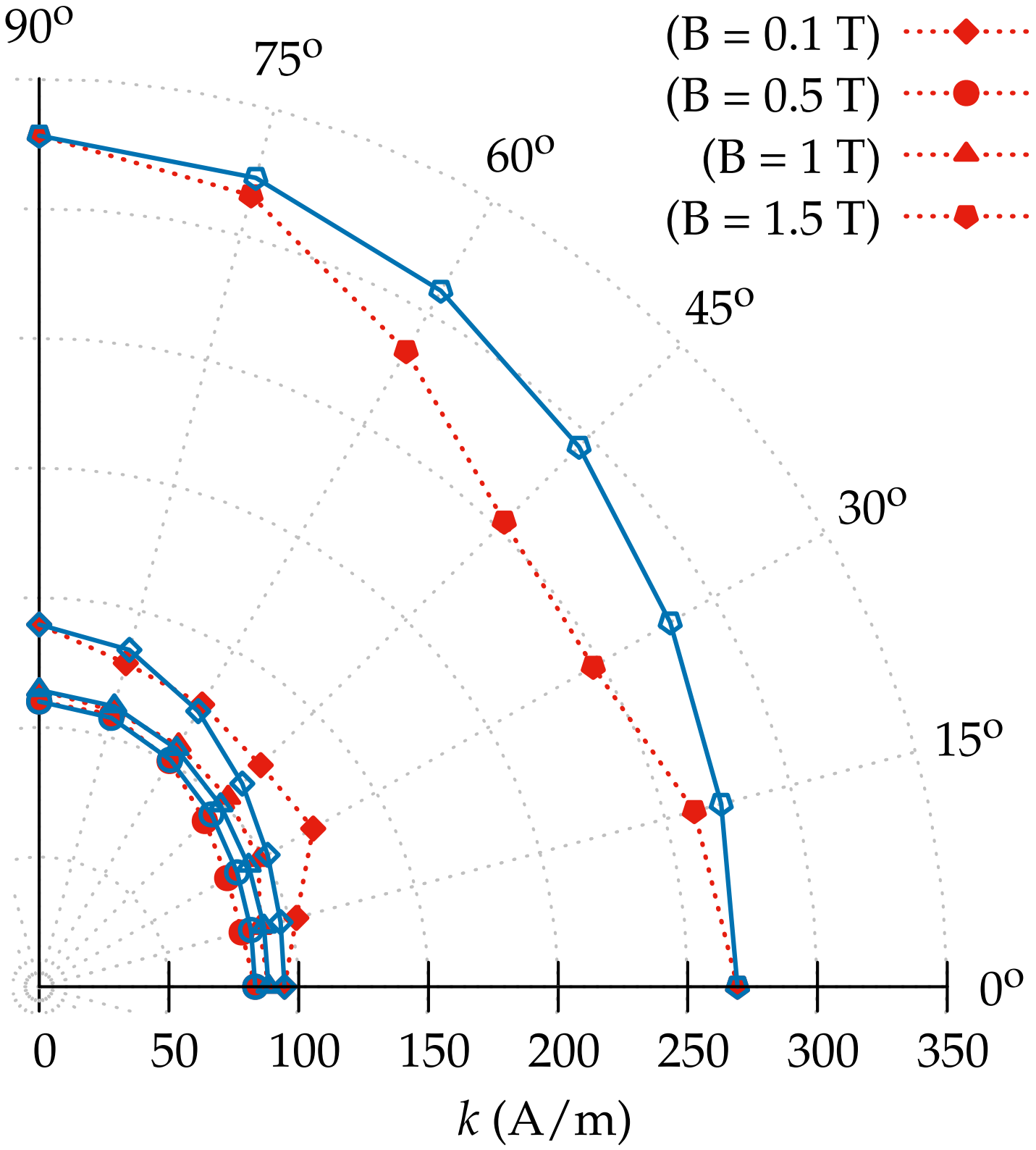
90°
75°
60°
45°
30°
15°
0°
(B = 0.1 T)
(B = 0.5 T)
(B = 1 T)
(B = 1.5 T)
0
50
100
150
200
250
300
350
k (A/m)

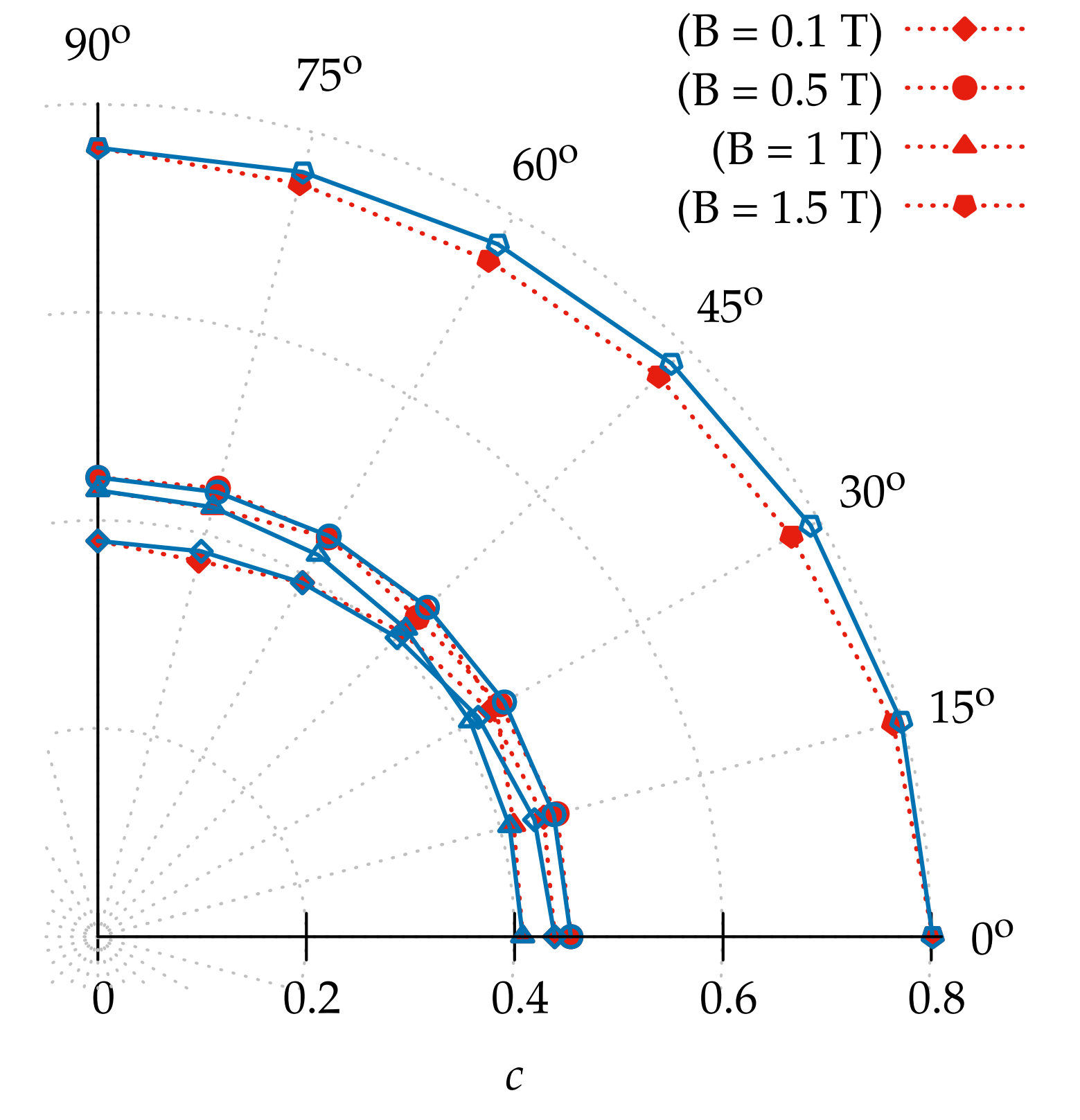
90°
75°
60°
45°
30°
15°
0°
(B = 0.1 T)
(B = 0.5 T)
(B = 1 T)
(B = 1.5 T)
0
0.2
0.4
0.6
0.8
c

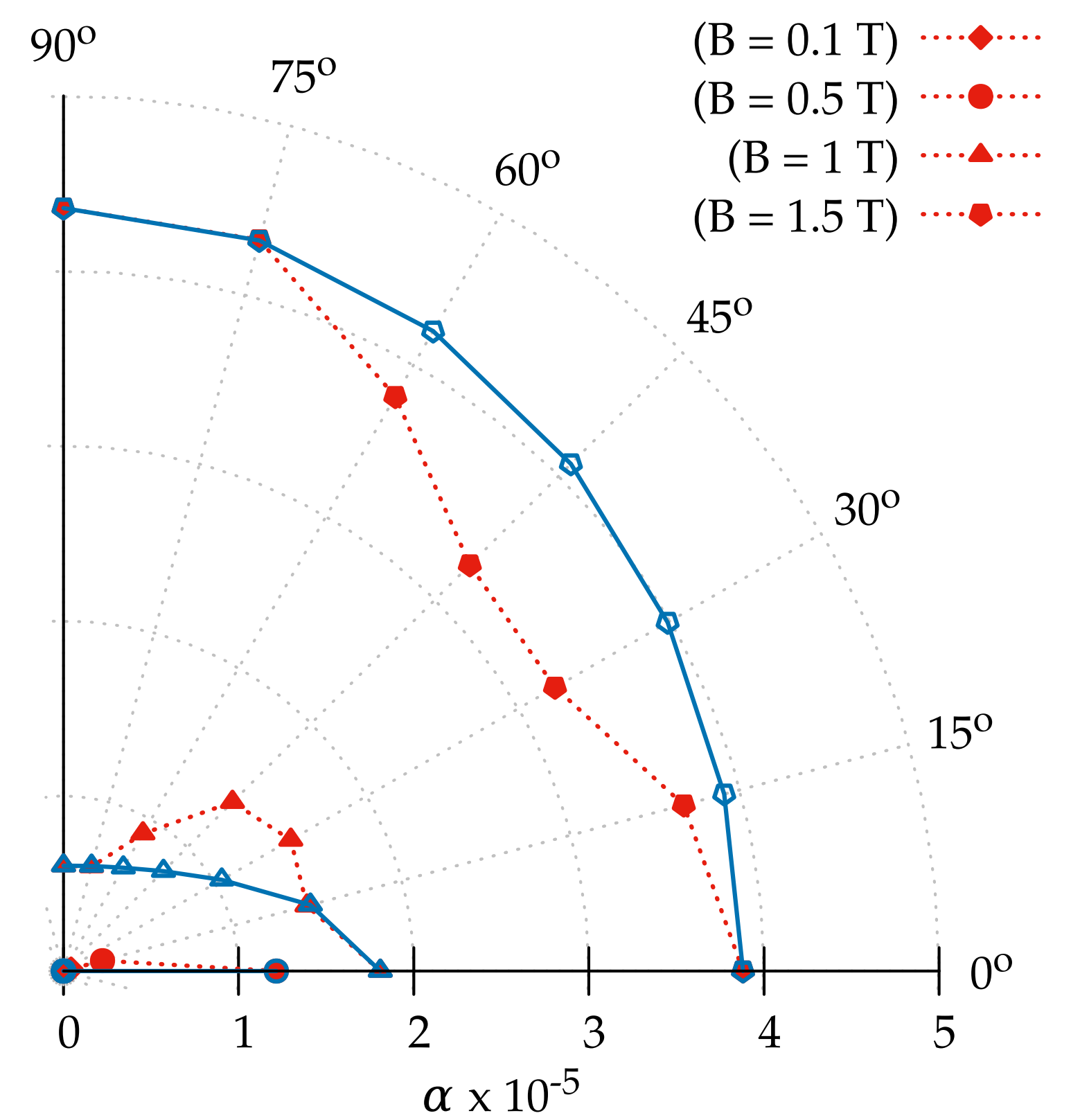
90°
75°
60°
45°
30°
15°
0°
(B = 0.1 T)
(B = 0.5 T)
(B = 1 T)
(B = 1.5 T)
0
1
2
3
4
5
α x 10-5

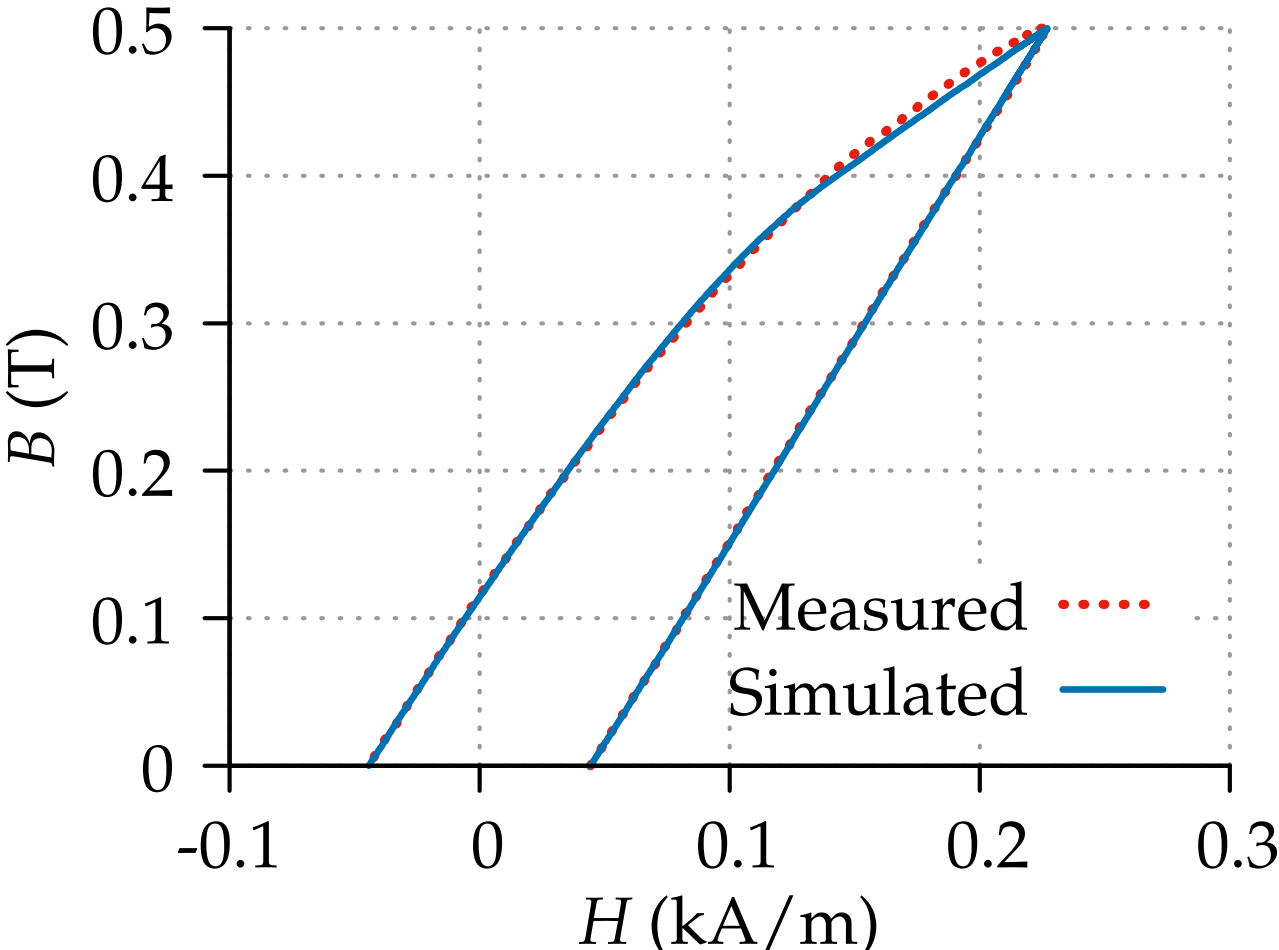
0.5
0.4
0.3
0.2
0.1
0
B (T)
-0.1
0
0.1
0.2
0.3
H (kA/m)
Measured
Simulated

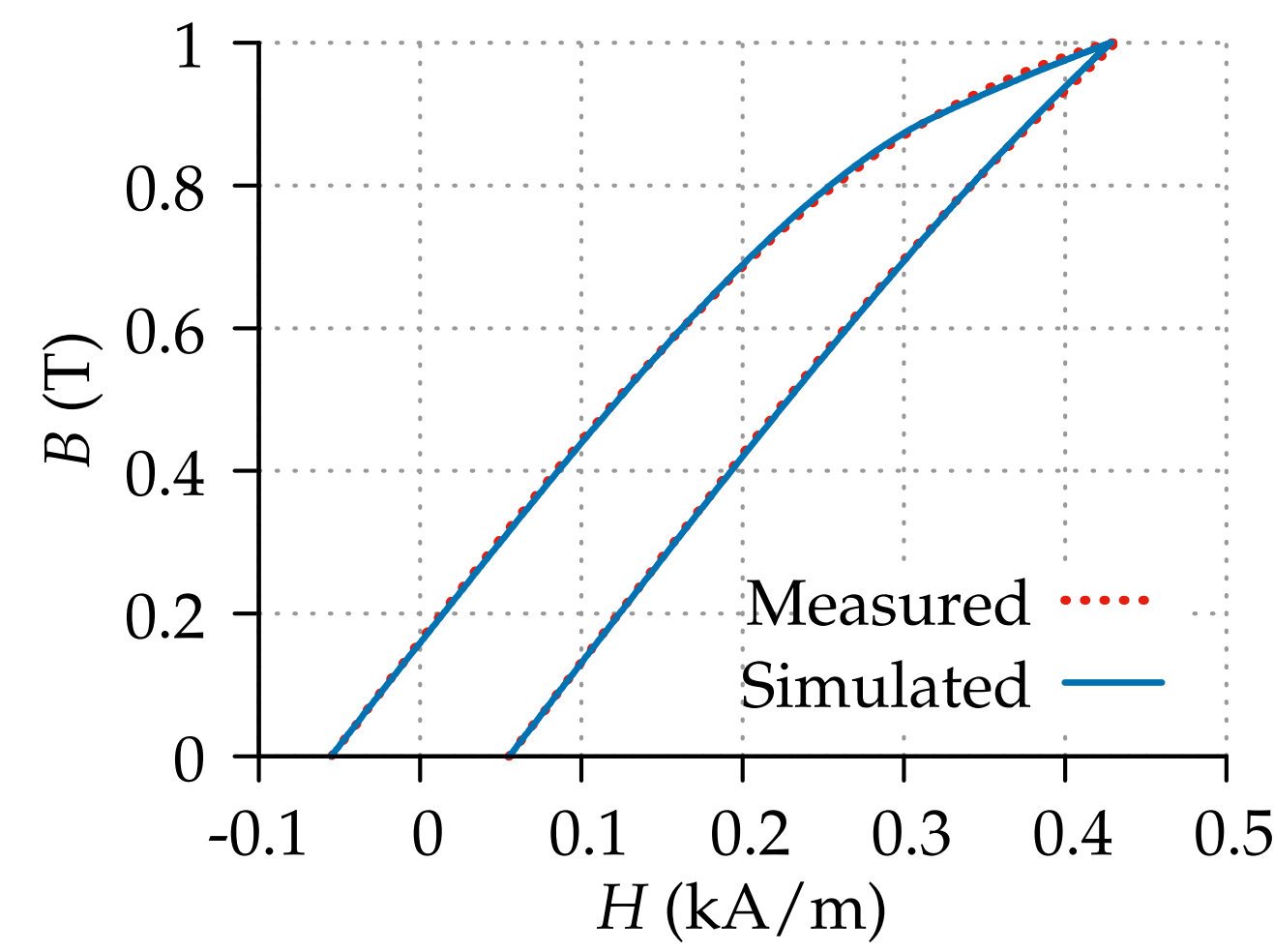
1
0.8
0.6
0.4
0.2
0
B (T)
-0.1
0
0.1
0.2
0.3
0.4
0.5
H (kA/m)
Measured
Simulated

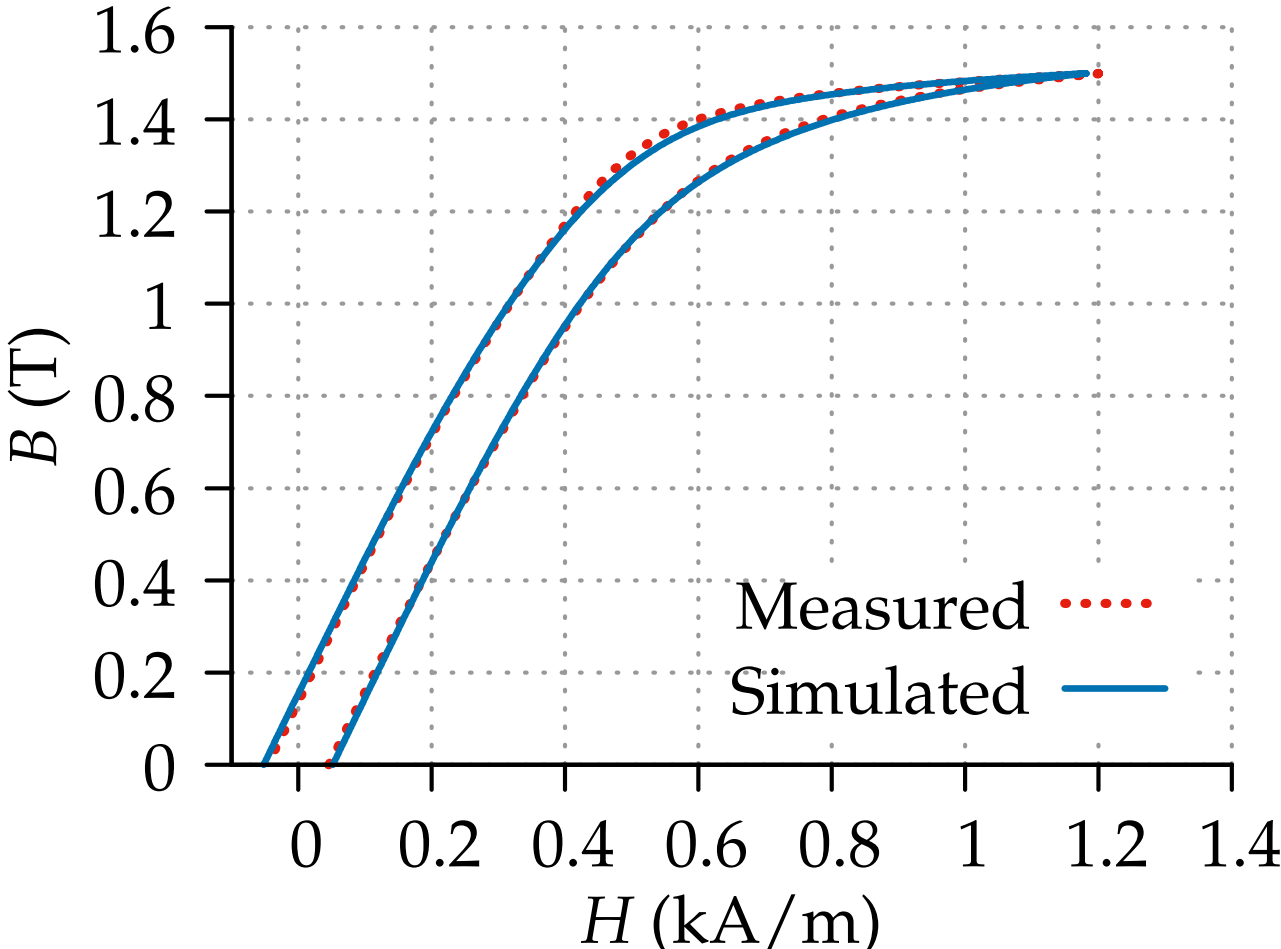
1.6
1.4
1.2
1
0.8
0.6
0.4
0.2
0
B (T)
0
0.2
0.4
0.6
0.8
1
1.2
1.4
H (kA/m)
Measured
Simulated

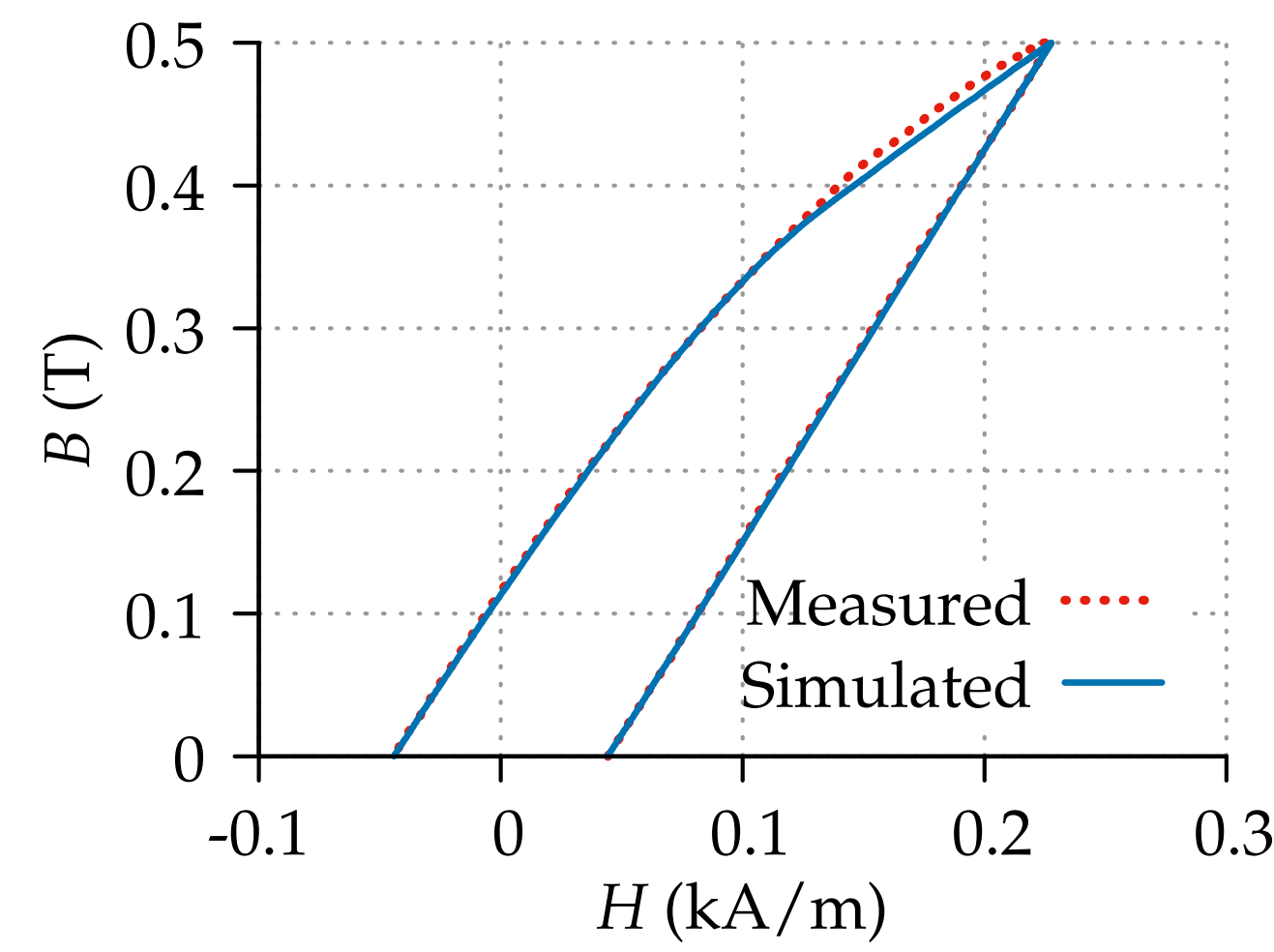
0.5
0.4
0.3
0.2
0.1
0
B (T)
-0.1
0
0.1
0.2
0.3
H (kA/m)
Measured
Simulated

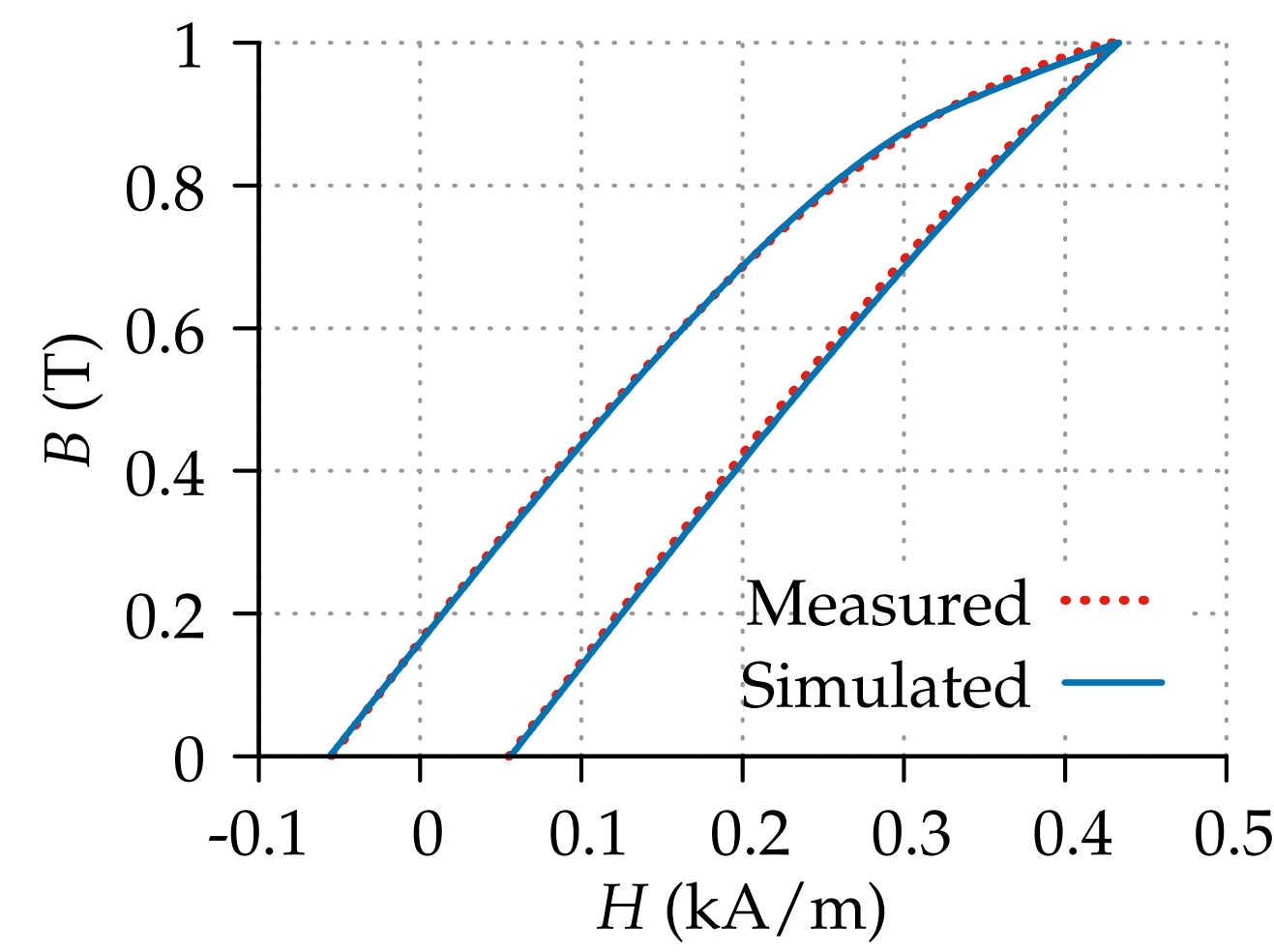
1
0.8
0.6
0.4
0.2
0
B (T)
-0.1
0
0.1
0.2
0.3
0.4
0.5
H (kA/m)
Measured
Simulated

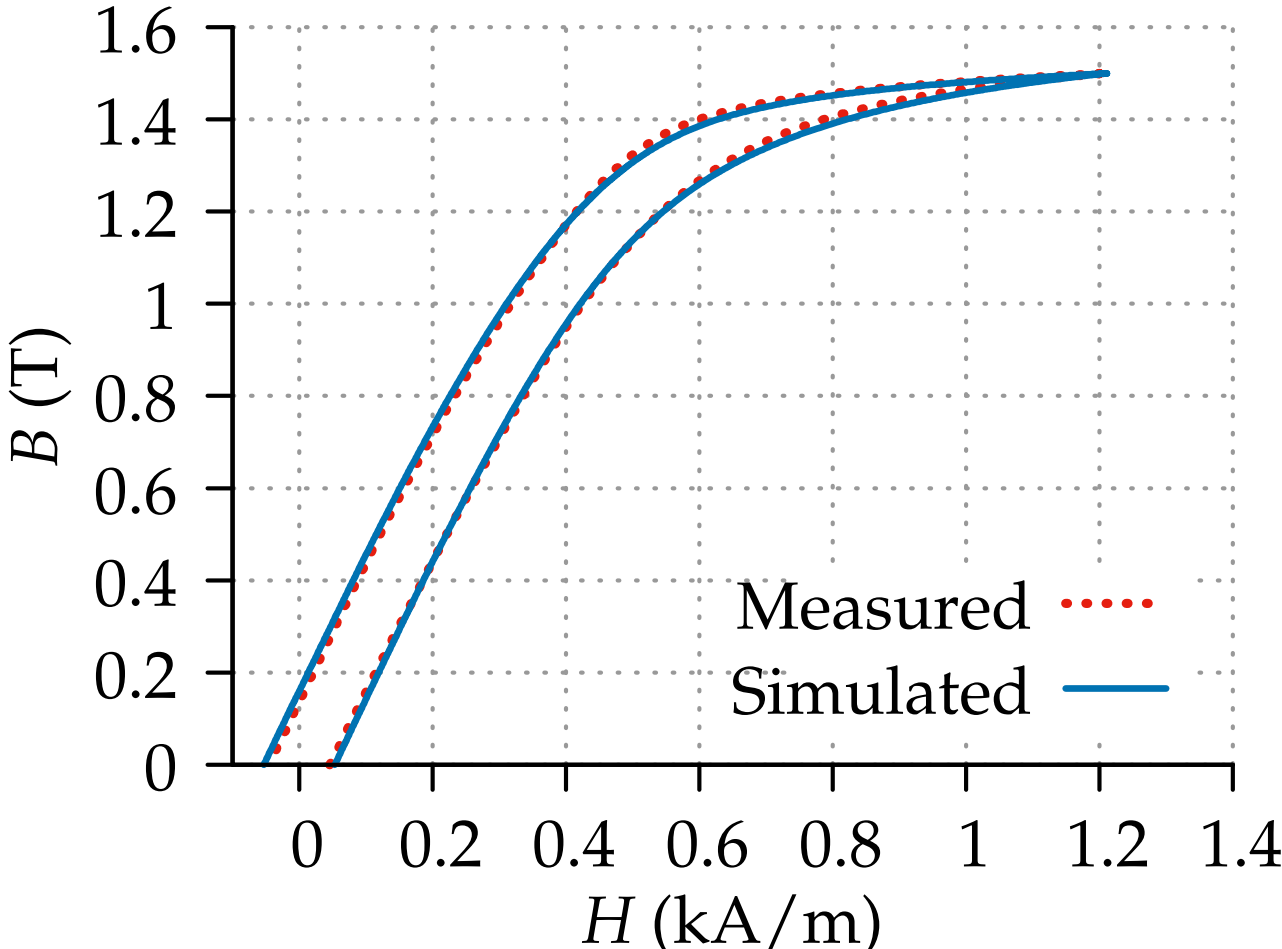
1.6
1.4
1.2
1
0.8
0.6
0.4
0.2
0
B (T)
0
0.2
0.4
0.6
0.8
1
1.2
1.4
H (kA/m)
Measured
Simulated

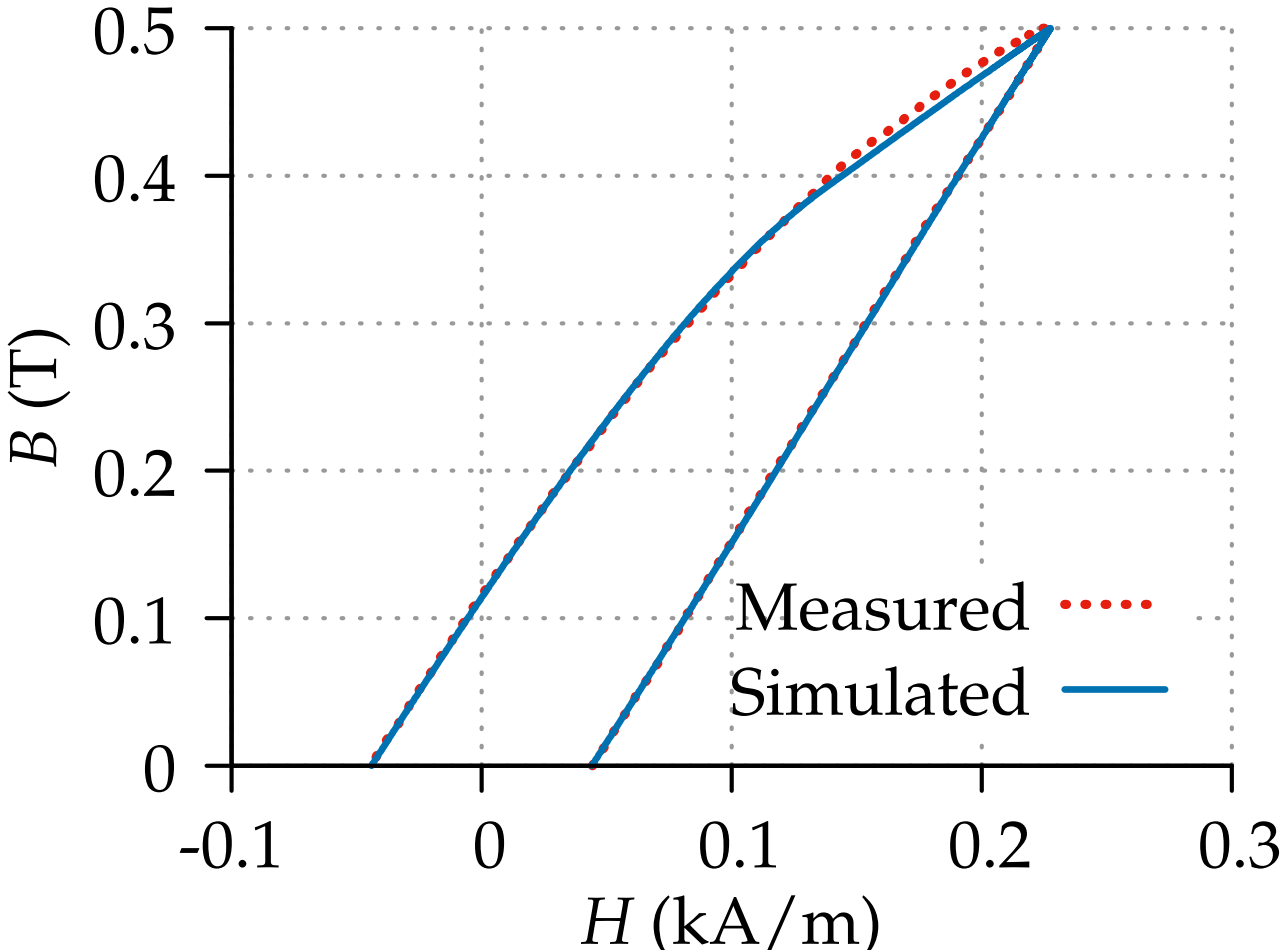
0.5
0.4
0.3
0.2
0.1
0
B (T)
-0.1
0
0.1
0.2
0.3
H (kA/m)
Measured
Simulated

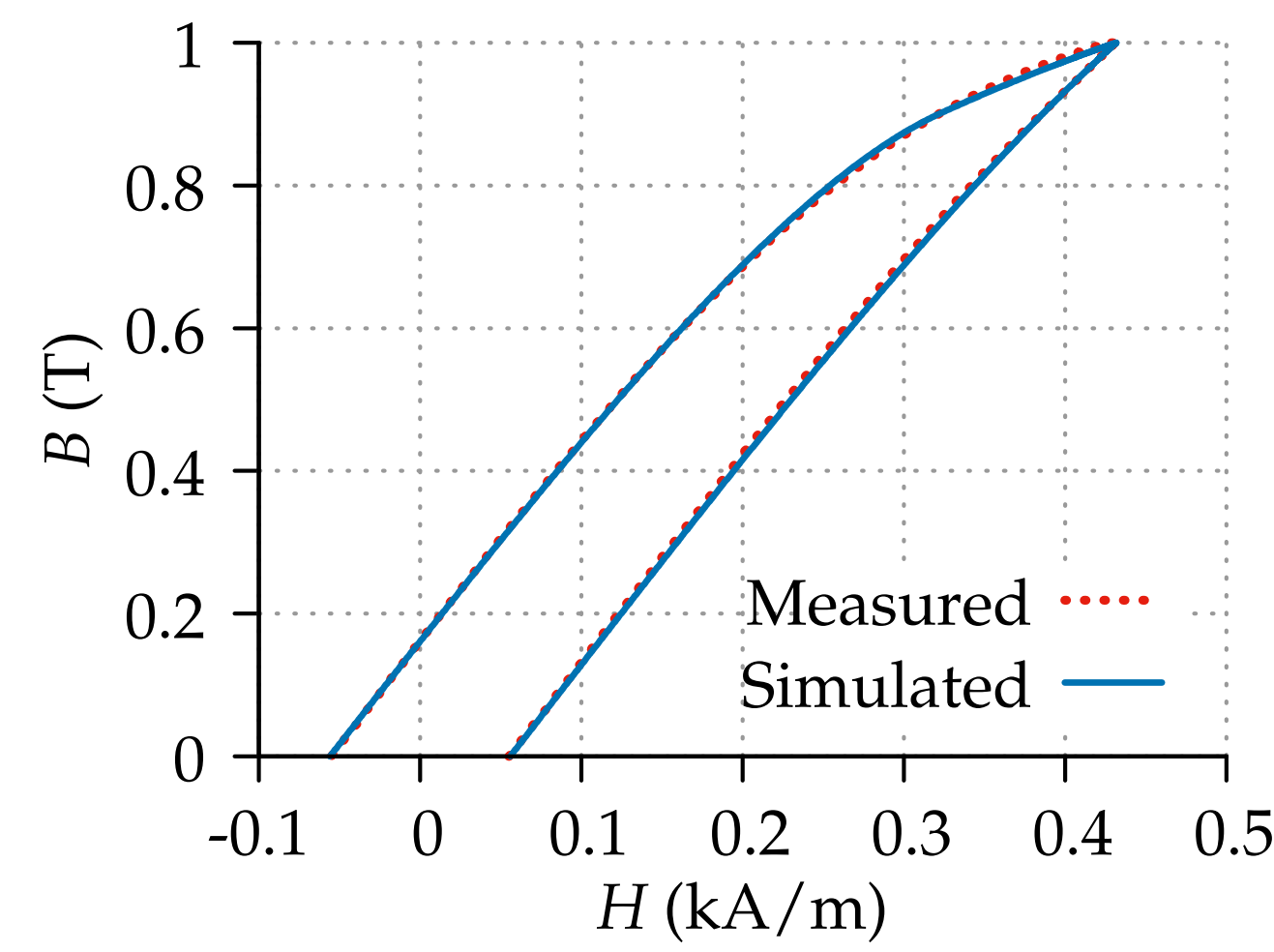
1
0.8
0.6
0.4
0.2
0
B (T)
-0.1
0
0.1
0.2
0.3
0.4
0.5
H (kA/m)
Measured
Simulated

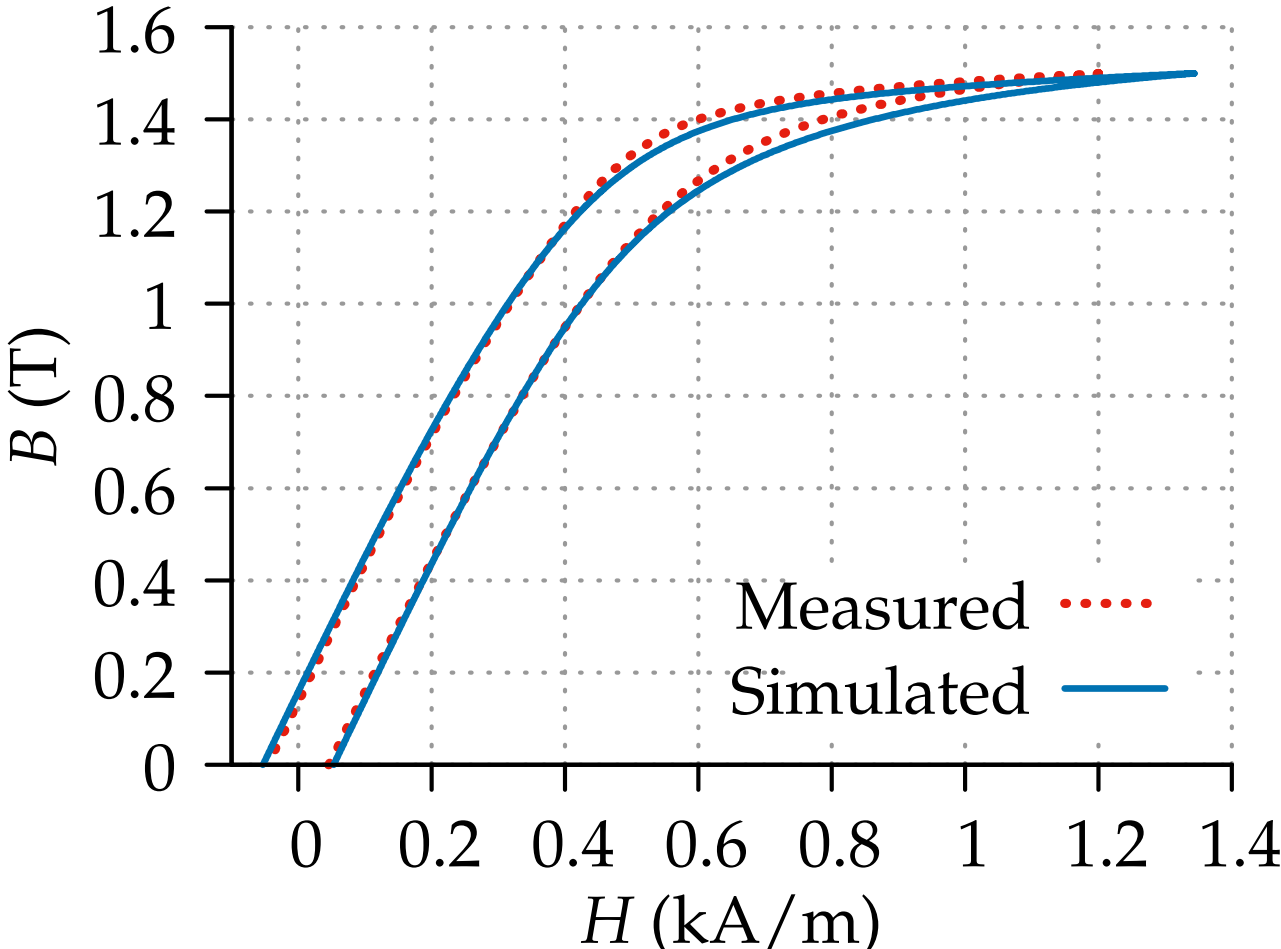
1.6
1.4
1.2
1
0.8
0.6
0.4
0.2
0
B (T)
0
0.2
0.4
0.6
0.8
1
1.2
1.4
H (kA/m)
Measured
Simulated

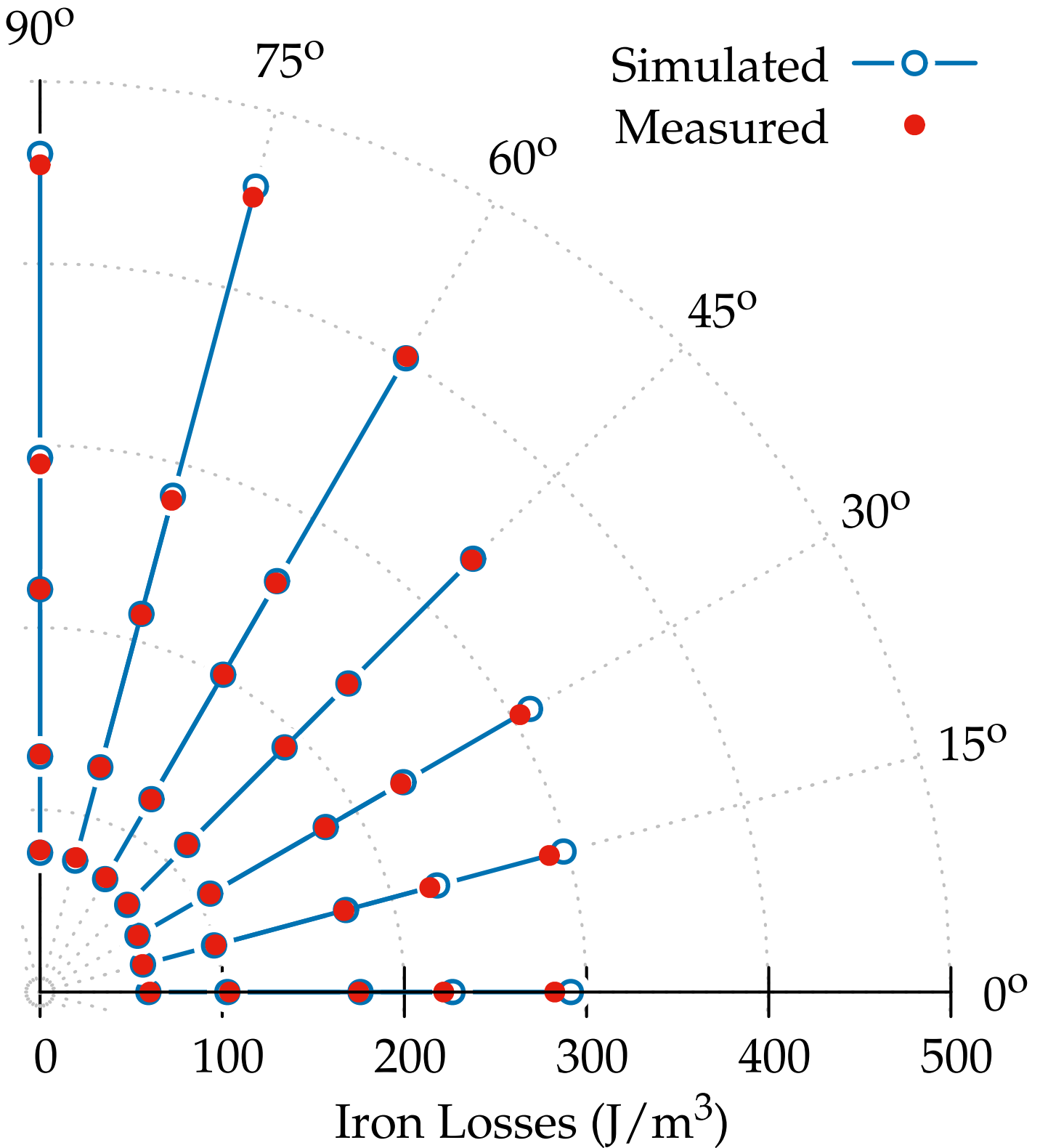
90º
75º
60º
45º
30º
15º
0º
Simulated
Measured
0
100
200
300
400
500
Iron Losses (J/m3)

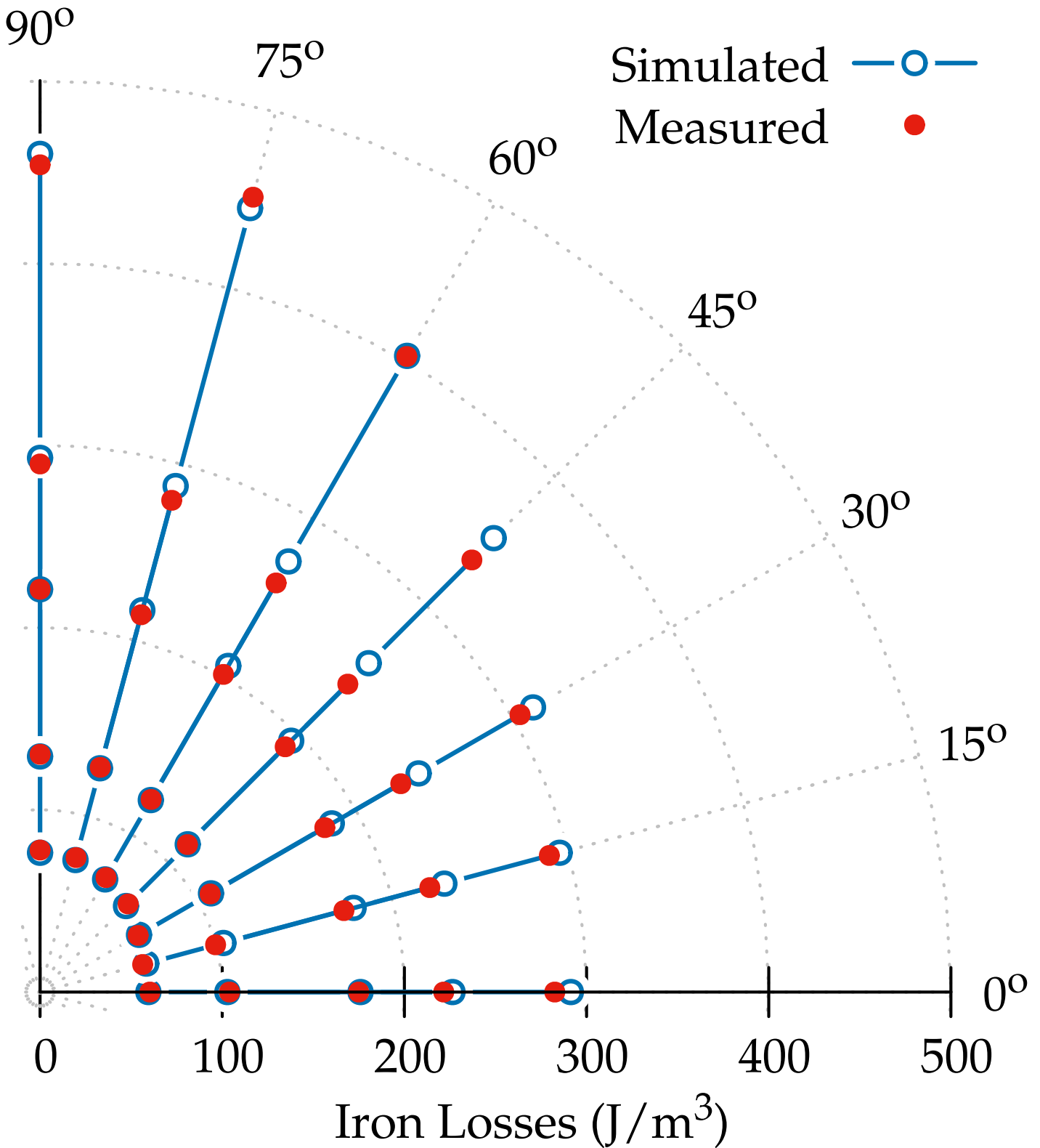
90º
75º
60º
45º
30º
15º
0º
Simulated
Measured
0
100
200
300
400
500
Iron Losses (J/m3)

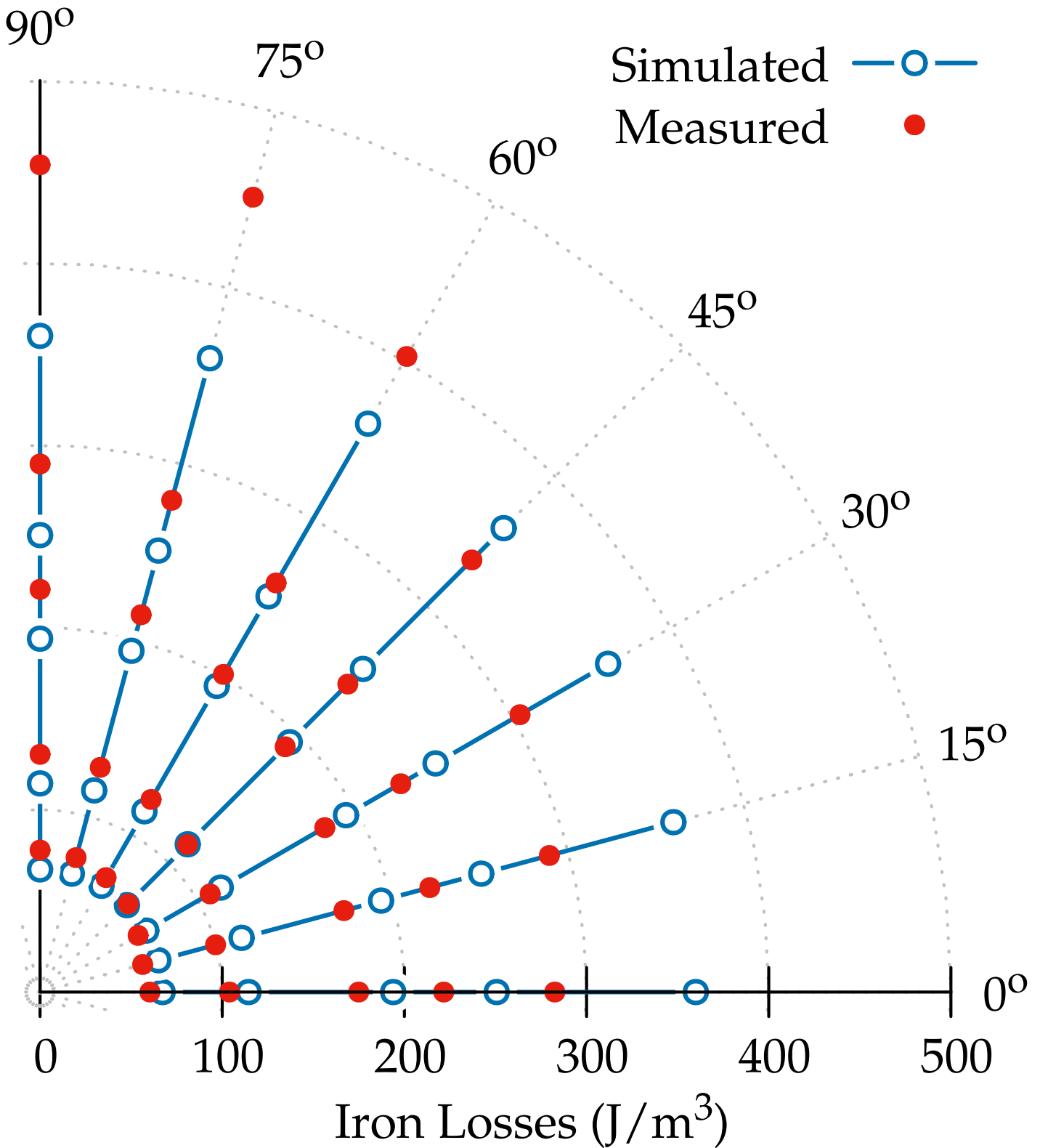
90º
75º
60º
45º
30º
15º
0º
Simulated
Measured
0
100
200
300
400
500
Iron Losses (J/m3)